REPORT DOCUMENTATION PAGE		Form Approved OMB No. 0704

1. AGENCY USE ONLY *(Leave blank)*	2. REPORT DATE December 1994	3. REPORT TYPE AND DATES COVER Master's Thesis
4. TITLE AND SUBTITLE OPERATIONAL TESTING AND THERMAL MODELING OF A TOPAZ-II SINGLE-CELL THERMIONIC FUEL ELEMENT TEST STAND		5. FUNDING NUMBERS
6. AUTHOR(S) Benke, Steven M.		
7. PERFORMING ORGANIZATION NAME(S) AND ADDRESS(ES) Naval Postgraduate School Monterey CA 93943-5000		8. PERFORMING ORGANIZATION REPORT NUMBER
9. SPONSORING/MONITORING AGENCY NAME(S) AND ADDRESS(ES)		10. SPONSORING/MONITORING AGENCY REPORT NUMBER
11. SUPPLEMENTARY NOTES The views expressed in this thesis are those of the author and do not reflect the official policy or position of the Department of Defense or the U.S. Government.		
12a. DISTRIBUTION/AVAILABILITY STATEMENT Approved for public release; distribution is unlimited		12b. DISTRIBUTION CODE

13. ABSTRACT *(maximum 200 words)*

A TOPAZ-II Thermionic Fuel Element (TFE) test stand is under study at the TOPAZ International Program. Extensive cross-sectional drawings of this system are presented along with detailed descriptions of its construction. A thermal analysis of the test stand is completed using a thermal resistance network method and data collected on the test stand. Critical resistances in the network include the 0.5 mm regulated helium gap, cooling water channel, and cesium interelectrode gap. The thermal analysis indicates that for an input power to the active zone of 3003 W, and a regulated helium gap pressure of 10 torr, the thermal conductivity of the regulated gap helium ranges from 0.073-0.087 W/mK. This is much less than the thermal conductivity calculated as a function of temperature only of 0.276 W/mK. For a mass flow rate of 0.04 kg/s, the convective heat transfer coefficients ranges from 528-1012 W/m^2K based on correlations for fully developed laminar and turbulent flow. This model may be used in conjunction with a thermionic emission model in order to more completely evaluate the operating characteristics of the test stand, and to better correlate results with actual operating conditions in the TOPAZ-II reactor core.

14. SUBJECT TERMS Thermionics, TOPAZ-II, Thermal Modeling			15. NUMBER OF PAGES 111
			16. PRICE CODE
17. SECURITY CLASSIFICATION OF REPORT Unclassified	18. SECURITY CLASSIFICATION OF THIS PAGE Unclassified	19. SECURITY CLASSIFICATION OF ABSTRACT Unclassified	20. LIMITATION OF ABSTRACT UL

OPERATIONAL TESTING AND THERMAL MODELING OF A TOPAZ-II SINGLE-CELL THERMIONIC FUEL ELEMENT TEST STAND

by

Steven M. Benke
Lieutenant, United States Navy
B.S, University of New Mexico, 1987

Submitted in partial fulfillment
of the requirements for the degree of

MASTER OF SCIENCE IN ASTRONAUTICAL ENGINEERING

from the

NAVAL POSTGRADUATE SCHOOL
December 1994

Daniel J. Collins, Chairman
Department of Aeronautics andAstronautics

iv

ABSTRACT

A TOPAZ-II Thermionic Fuel Element (TFE) test stand is under study at the TOPAZ International Program. Extensive cross-sectional drawings of this system are presented along with detailed descriptions of its construction. A thermal analysis of the test stand is developed using a thermal resistance network method and data collected on the test stand. Critical resistances in the network include the 0.5 mm regulated helium gap, cooling water channel, and cesium interelectrode gap. The thermal analysis indicates that for an input power to the active zone of 3003 W, and a regulated helium gap pressure of 10 torr, the thermal conductivity of the regulated gap helium ranges from 0.073-0.087 W/mK. This is much less than the thermal conductivity calculated as a function of temperature only of 0.276 W/mK. For a water mass flow rate of 0.04 kg/s, the convective heat transfer coefficient ranges from 528-1012 W/m^2K based on correlations for fully developed laminar and turbulent flow. Our model may be used in conjunction with a thermionic emission model in order to more completely evaluate the operating characteristics of the test stand, and to better correlate results with actual operating conditions in the TOPAZ-II reactor core.

TABLE OF CONTENTS

LIST OF FIGURES

ACKNOWLEDGMENT

Last, but not least, a big thanks goes to my friend and colleague Rich Venable. His help on investigating and developing the ground-work for this thesis, as well as his continual help throughout the thesis process, was needed and greatly appreciated.

I. INTRODUCTION

The TOPAZ-II Thermionic Fuel Element (TFE) test stand was originally built and tested at the Scientific Industrial Association "LUTCH" in Podolsk, Russia. In December, 1992, the stand was reassembled at the New Mexico Engineering Research Institute (NMERI) in Albuquerque, New Mexico. The TFE test stand was designed to conduct single TFE non-nuclear testing by replacing the nuclear fuel with a tungsten heating element (TISA heater). The test stand provides a means to test a single TFE so that its performance can be better observed without the interference and complexity of the integrated TOPAZ-II system. This removes the direct coupling of the TOPAZ-II in-core TFE with the coolant loop, radiator and the other TFEs electrically connected in series. Acceptance and demonstration testing were conducted throughout 1993 (Luchau et al., 1993).

In order to better understand and predict the behavior of a TFE in the test stand, a detailed thermal analysis based on a network method needs to be developed to account for the thermal losses in the stand. Because of the large amounts of Russian technical data and engineering drawings associated with the TOPAZ-II TFE test stand, and due to the extreme difficulty in translating Russian technical information, the implementation of this thermal model required the creation of detailed and extensive cross-sectional drawings for this thesis. *Mathcad Plus 5.0* (MathSoft, Inc., 1994) was the primary technical calculation software used to solve the thermal analysis model.

Since the test stand provides a means for testing a single TFE without the support of the supporting TOPAZ-II reactor systems, there are several differences in the construction and operation of the test stand from the TOPAZ-II reactor core. In the test stand, water cooling is used to remove the excess heat instead of the liquid metal cooling

1

that is used in the reactor core. The cooling water flows through the test stand water jacket along a torturous path to aid in its heat removal ability. The heat transfer coefficient for the cooling water is directly dependent on the flow cross-sectional area and the total heat transfer area, both of which are challenging to determine. Thermocouples internal to the test stand provide a axial temperature distribution along the TFE working section. No internal temperature measurements are made in the TOPAZ-II reactor core TFEs. Heaters are also located internally in the test stand to provide a means of degassing the test stand components prior to operation. A 0.5 mm gap in the test stand just inside of the cooling water jacket is filled with low pressure helium to provide a means of controlling the heat transfer through the test stand. This gap is used to help the test stand better simulate the operating conditions experienced by a TFE in the reactor core. Due to the low pressure band that the gap is adjusted over (from 1 to 10 torr), the pressure dependence of the rarefied helium's thermal conductivity is difficult to define.

Experimental data for this work were collected in March 1994, with follow-on experimental data taken in August 1994 at NMERI. Along with aiding in the development of the thermal model for the test stand, these data are used to investigate several of the critical resistances from the thermal network. A good understanding of the test stand thermal characteristics is essential in evaluating the performance of a single TFE operating in the test stand, and correlating that performance to a TFE operating in the TOPAZ-II reactor core. The experimentally measured input power to the TFE working section along with the collector sleeve temperature information is also used as an input to the TOPAZ-II Thermionic Transient Analysis Model (TITAM). TITAM is a computer simulation program developed by the University of New Mexico to look at both steady-state and transient operating characteristics of the TOPAZ-II reactor system (Paramonov ·and El-Genk, 1994).

2

The goals of this work include the creation of detailed engineering drawings for the test stand, investigation of test stand material properties, development of a thermal model for the test stand, and benchmarking the model with the experimental data collected. Additionally, experimental data are used to empirically fix a range for several of the thermal properties that cannot be easily determined.

LT J. R. Venable is writing a companion thesis that will concentrate on the thermionic theory behind the data collected for this thesis. Venable's thesis will be available after March of 1995 and a joint paper will be presented ("Operational Testing and Thermal Modeling of a TOPAZ-II Single-Cell Thermionic Fuel Element Test Stand") at the Space Nuclear Power and Propulsion Symposium held in Albuquerque, New Mexico, on January 8-12, 1995.

II. BACKGROUND

The continued exploration and exploitation of space will require increasing amounts of power as technology continues to advance. Supporting high definition television broadcasts and the rapidly growing world-wide communication needs, moving large level research and industrial opportunities to Earth orbit or into the cislunar region, revisiting and colonizing the Moon, and pushing the envelope of civilization to Mars and beyond are future goals which will demand large electrical power sources that are both compact and have long lifetimes. These larger power sources will need to survive harsh environments, including radiation belts, the vacuum of deep space, and hostile atmospheres of other planets and natural satellites in the solar system. Nuclear power can provide the compact power sources necessary to meet these future needs.

A. UNITED STATES SPACE NUCLEAR POWER PROGRAMS

Since the mid-1950s, the United States has been interested in the use of nuclear power in space applications. From radioisotope power systems, nuclear rockets, and the use of nuclear reactors for power production, interest in the space nuclear power area was motivated by a favorable political environment and public support until the early 1970s.

The Transit 4A navigational satellite was launched in June of 1961 with a SNAP-3B Radioisotope Thermoelectric Generator (RTG) to provide power. Since that first successful launch of a nuclear power source, a total of 24 launches using RTGs have followed including the Pioneer, Viking, and Voyager missions. Although the RTG has proved to be very useful for many applications, the ability to support a very ambitious space program required the development of a nuclear reactor based on the principle of atomic fission for both propulsion purposes and to provided electrical power.

Project Rover was initiated at Los Alamos National Laboratory in 1955 and was the beginning of approximately 18 years of research and development into nuclear rockets. Although the nuclear rocket program was terminated in late 1972, it was the start of the search for a high temperature nuclear reactor. The research and demonstration test of the Nuclear Engine for Rocket Vehicle Application (NERVA) program proved that a nuclear reactor could provide a high power density rocket with high thrust and specific impulse. (Angelo and Buden, 1985)

Active development of a nuclear reactor to provide electric power began in 1957 with the Systems for Nuclear Auxiliary Power (SNAP) program. These nuclear reactors required a power generation method to convert the heat created by atomic fission into electrical power. The initial concept was SNAP-2, a thermal uranium zirconium-hydride reactor that utilized a Rankine cycle with mercury as the working fluid to convert the nuclear heat to electricity. This was the precursor to two separate concepts, the SNAP-8 and the SNAP-10A, both of which were initiated in 1960. The SNAP-8 reactor utilized a mercury Rankine cycle along with a larger version of the SNAP-2 reactor system to support anticipated higher power demands. (Angelo and Buden, 1985)

The SNAP-10A was also based on the SNAP-2 reactor system, but instead of using the dynamic Rankine power conversion cycle, it used a thermoelectric power conversion system. The use of static power conversion provides a means of converting heat directly into electricity without the need of a secondary working fluid (such as mercury for a Rankine cycle or helium-xenon for a closed Brayton cycle) and the associated turbines and pumps/compressors. In April of 1965, the SNAPSHOT mission was successfully launched carrying a SNAP-10A reactor to approximately a 1300 km orbit. Although the SNAP-10A reactor shutdown only 43 days after becoming critical, it proved that a nuclear reactor could be successfully launched and operated on orbit. This

was the only attempt by the United States to launch a nuclear reactor into space. (Angelo and Buden, 1985)

Another static power conversion method that was developed in parallel with the thermoelectric method was thermionic power conversion. Whereas thermoelectrics work on the basis of a thermally induced emf at the junction of two dissimilar semiconductors, thermionics works basically by "boiling off" electrons from a hot emitter surface and collecting the electrons on a relatively cooler collector surface across a small gap. The collector and emitter are then electrically connected together through an external load which completes the electrical circuit. The process of thermionics is discussed in more detail in the next chapter. Although thermionic devices were tested in the mid- to late-1960s, no complete reactor systems using thermionics was actually built in the United States. (Angelo and Buden, 1985)

Due to a changing political environment and shifting emphasis in the space program, all nuclear reactor development programs were canceled at the end of 1972. Although some research did continue after 1972, it wasn't until the early 1980s that increased interest was returned to space nuclear reactors. This renewed interest was mainly due to the need for a large power source to support the Strategic Defense Initiative (SDI). The advance space nuclear power program was reinitiated as the Space Power Advanced Reactor (SPAR) system later renamed SP-100. Several reactor designs and power conversion systems were initially considered for SP-100. The primary concept that SP-100 developed utilized a thermoelectric power conversion system. (Angelo and Buden, 1985) Research on SP-100 has continued until 1994 when once again the political environment has changed and funding for the program is being terminated.

B. FORMER SOVIET UNION SPACE NUCLEAR POWER PROGRAMS

The former Soviet Union, like the United States, was very active in the research and development of space nuclear power. From the early 1960s to 1989, a total of 38 nuclear reactor systems were launched by the former Soviet Union. The majority of the nuclear reactors launched were for the Radar Ocean Reconnaissance SATellites (RORSATs) and utilized thermoelectric energy conversion. The other two nuclear reactors launched were COSMOS-1818 and COSMOS-1867. Both COSMOS satellites were test platforms for the TOPAZ-I reactor system utilizing multi-cell thermionic energy conversion. (Polansky et al., 1994)

In the early 1960s, the former Soviet Union began development of single-cell and multi-cell TFEs. In 1967 the two concepts were sent for system development to two separate technical institutes. The single-cell TFE was developed by the Central Design Bureau of Machine Building (CDBMB) in St. Petersburg under the project name of ENISY. The multi-cell TFE was developed by the Scientific and Production Cooperation "Krasnaya Zvezda" in Moscow under the project name of TOPAZ, the Russian acronym for Thermionic Experiment with Conversion in Active Zone. Both concepts were developed cooperatively between the two institutes up until the early 1970s. This lead to many similarities between the two reactor designs. Cooperative efforts ended in the early 1970s due to differences between the two institutes and the programs developed independently. (Voss, 1994)

In 1987 and 1988, the multi-cell TFE reactor TOPAZ was successfully launched twice on COSMOS-1818 and COSMOS-1867. The first mission operated for 142 days and the second mission operated for 342 days before the planned depletion of the cesium supplies on board terminated the tests. Both test were extremely successful and confirmed that the on-orbit data correlated well to ground test results. (Paramonov and El-Genk,

1994) Although there were 26 single-cell TFE ENISY reactor systems manufactured and 19 systems tested between 1970 and 1989, none of the single-cell TFE technology were ever launched and tested on orbit. (Schmidt et al., 1994)

C.   TOPAZ INTERNATIONAL PROGRAM

At the end of the 1980s, the Russians approached a private U.S. company (International Scientific Products, San Jose, CA) about transferring Russian thermionic technology through the purchase of Russian space reactor hardware. During the negotiations, the U.S. company inadvertently renamed ENISY to TOPAZ-II and TOPAZ to TOPAZ-I (Voss, 1994). In May of 1992, the U.S. Government purchased two complete TOPAZ-II reactor systems and associated test and support hardware through the purchasing agent International Scientific Products. Funding was provided by the Strategic Defense Initiative Organization (SDIO) to investigate the possible use of the TOPAZ-II reactor system in support of the Nuclear Electric Propulsion (NEP) Space Test Mission. This project has since been named the Topaz International Program (TIP). (Wyant, 1994)

The TIP facility is located at NMERI which is owned and operated by the University of New Mexico in Albuquerque, NM. Funding is still being provided by the former SDIO (now the Ballistic Missile Defense Organization, BMDO) and administered by the U.S. Air Force's Phillips Laboratory. The New Mexico alliance for Thermionics which includes the University of New Mexico, Sandia National Laboratories and Los Alamos National Laboratory provides research support for the TIP program. The international effort includes scientist and engineers from the Russia, England, and France. Although the flight program for TIP has been canceled, in March of 1994 four additional TOPAZ-II units were purchased for continuing research into thermionics and reactor operation. (Wyant, 1994)

III. THERMIONIC ENERGY CONVERSION

A.   BASIC THEORY

The thermionic process can be considered to be a "heat engine" which utilizes electrons as its working fluid to convert heat into electricity. The thermionic converter consists of a emitter, collector, and a small gap between the two. The collector is electrically connected to the emitter through an external load to complete the electrical circuit. Figure 3-1 shows a simplified flat-plate thermionic converter (Rasor, 1991). Electrons are "boiled" off the hot emitter and travel across the gap and are "condensed" on
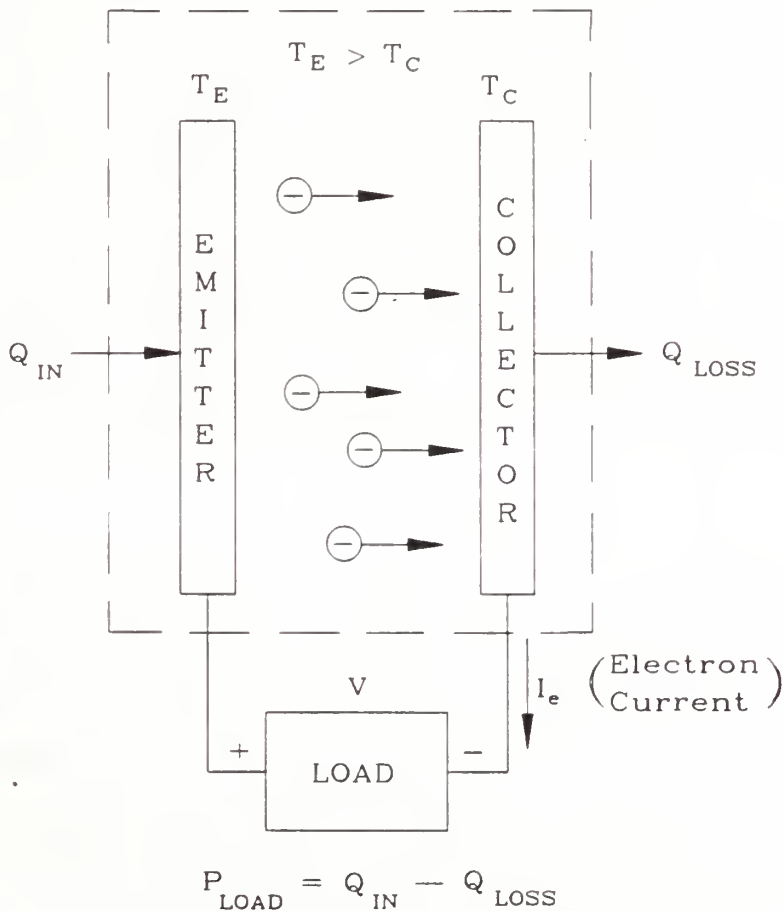
Figure 3-1. Simplified Flat-plate Thermionic.

11

the relatively cooler collector. The potential difference between the emitter and collector creates a driving force which causes a current to flow through the external load. (Angelo and Buden, 1985)

Since the thermionic device acts as a "heat engine," the maximum efficiency of the thermionic cycle can be characterized as the cycles Carnot efficiency. Some of the inefficiencies of the thermionic cycle include: (1) radiation heat transfer from the emitter to the collector; (2) negative space charge in the gap that interferes with the electron flow from the emitter to the collector; and (3) thermal losses. These inefficiencies prevent the thermionic cycle from approaching Carnot cycle efficiency. (Angelo and Buden, 1985)

Radiation heat transfer from the emitter to the collector cannot be mitigated. Higher collector temperatures would not only reduced the amount of radiation heat transfer but would also allow for a much smaller radiator since the radiators surface area is inversely proportional to the radiators operating temperature to the fourth power. However, as the collector temperature increases, the number of electrons being "boiled" off the collectors surface, called electron back emission, also increases. This in effect causes the overall cycle efficiency to decrease dramatically. A design trade-off must be made to understand the optimum collector operating temperature. (Angelo and Buden, 1985)

The negative space charge in the gap can be decreased by either making the gap size smaller or by injecting a low pressure gas into the gap. A vacuum diode is a thermionic device that relies on a very small gap between the electrodes to reduce the current inhibiting effects of the electric field produced by the negative space charge. Theoretical spacing needed to produce useful current density approaches the associated Debye length (~ 1 μm) which is for a practical purpose very difficult to manufacture and maintain. This very narrow gap can be widened somewhat (up to at most 0.5 mm) by injecting a gas plasma into the gap. This type of thermionic device is known as a plasma

12

diode. The primary purpose of this plasma is to facilitate to transfer of electrons through the gap while minimizing the potential drop and current attenuation due to the presence of the plasma. (Rasor, 1991)

The most common gas that is used in this type of diode is cesium which has the lowest ionization potential of any chemical element (Angelo and Buden, 1985). A measure of the amount of energy necessary for a electron to escape through the potential barrier associated with the surface of a metal is called the work function and is given in units of electron-volts (eV) (Angrist, 1976). Not only does the cesium plasma in the gap decrease the space charge, it also may have the effect of forming a monolayer of cesium on both the emitter and collector causing a decrease in their associated work functions. This decrease in the metals work function is directly related to the pressure of the cesium in the gap and the electrode temperature. Cesium pressure can be controlled by adjusting the temperature of the liquid cesium reservoir which in effect controls the vapor pressure of the evaporating cesium. (Angelo and Buden, 1985)

B.   TOPAZ-II NUCLEAR REACTOR

The TOPAZ-II nuclear reactor consists of 37 individual TFEs incorporated in a cylindrical core arrangement. Figure 3-2 shows a cross-sectional view of the TOPAZ-II reactor. Each of 37 TFEs consist of a UO_2 fuel assemble, a single-cell cylindrical thermionic device, and a sodium-potassium (NaK) liquid metal cooling channel. Electrical power is supplied to the loads by 34 of the TFEs connected in series. These TFEs are designed to produce 5-6 kW_e at 27 VDC for up to 3 years. The other three TFEs are connected in parallel to provide power to the electromagnetic pump. This pump is used to generate the pumping power necessary to circulate the NaK. The overall length of the reactor core is 37.5 cm with an overall width of 26.0 cm. (Paramonov and El-Genk, 1994)

13
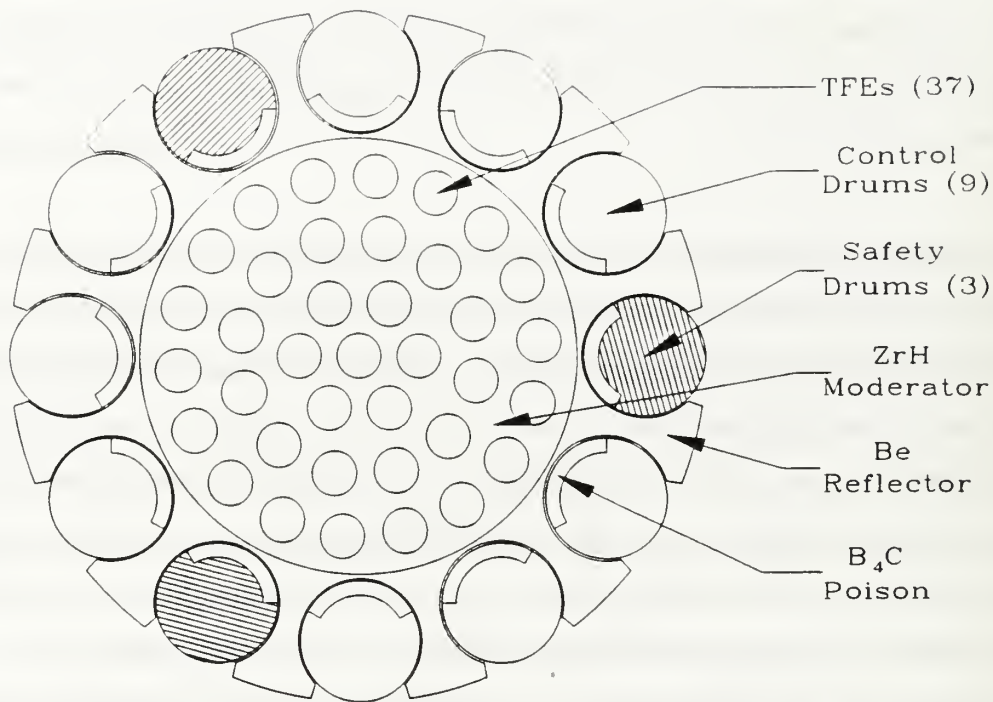
Figure 3-2. Cross-sectional View of the TOPAZ-II.

The TFEs are inserted into axial channels in a zirconium-hydride (ZrH) moderator. Twelve reflector drums surround the core, three are safety drums which are turned out prior to initial criticality when on orbit. The other nine reflector drums are used to control the nuclear reaction during operation and are called control drums. All of the reflector drums are made out of beryllium clad in stainless steel with a small section of neutron absorbing material made of boron-carbide (B_4C). A beryllium reflector surrounds the remainder of the core as shown in Figure 3-2. (Schmidt et al., 1994)

Excess heat is removed from the TFEs using a eutectic NaK coolant pumped through stainless steel piping by the electromagnetic pump. The hot coolant flows through a conical radiator where the waste heat is rejected to space. During normal operation the thermionic emitter temperature ranges between 1800 K to 2100 K and the NaK coolant maintains the collector temperature between 743 K to 843 K. (Schmidt et al., 1994)

14

C.   TOPAZ-II THERMIONIC FUEL ELEMENT

The TOPAZ-II TFE consists of a single-cell cylindrical thermionic converter. A single-cell converter utilizes the entire length of the reactor core as a single device. This is in contrast to the TOPAZ-I TFE which is made up of multi-cell thermionic converters. A simple comparison of the electrical circuit for both a single-cell and multi-cell TFE are shown in Figure 3-3. The advantages of using multi-cell converters are that they produce a higher power density and higher conversion efficiency. This is mainly due to less ohmic losses in the multi-cell because of the shorter thermionic elements. Another advantage of the multi-cell design is that each of the cells are connected in series resulting in a TFE output voltage in the volt range. This reduces the amount of electrical losses in the leads and makes the power distribution system more efficient. (Paramonov and El-Genk, 1994)
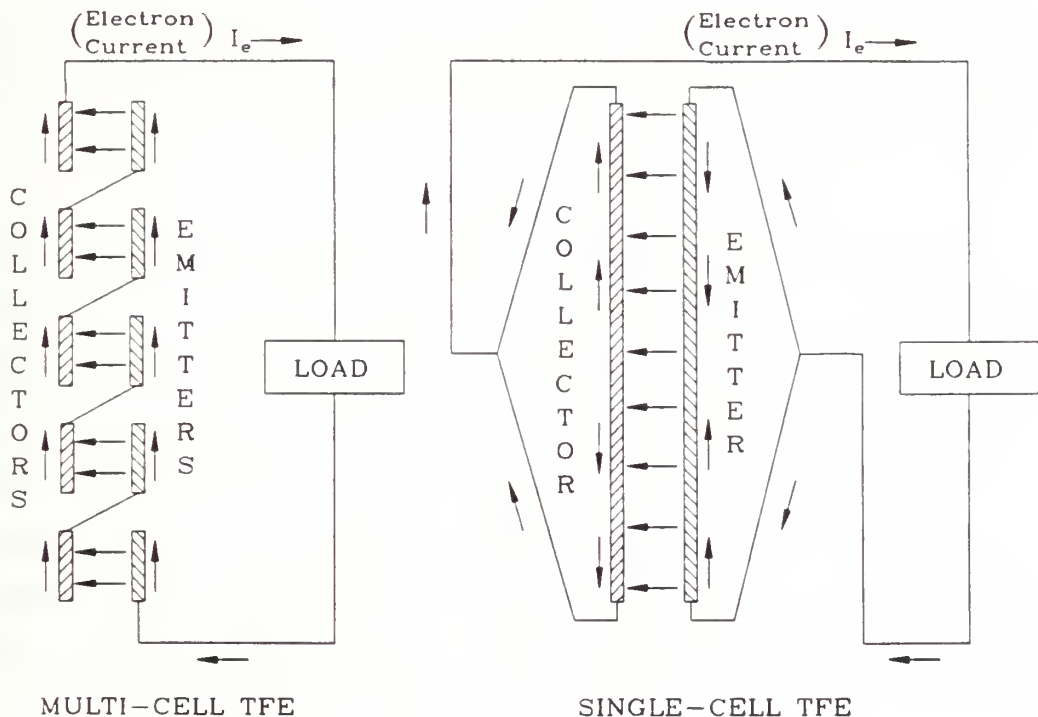
Figure 3-3. Simplified Electrical Schematics for Multi-Cell and Single-Cell TFEs.

The two major disadvantages of using a multi-cell TFE are that manufacturing is significantly more complicated and the design does not provide a means of removing the nuclear fuel and performing non-nuclear testing. Although the single-cell TFE design has a much lower efficiency, it does provide a less complicated converter and a means of performing non-nuclear testing. This testing is accomplished by replacing the UO_2 fuel assembly with a tungsten heater (TISA heater). (Paramonov and El-Genk, 1994) The TISA heaters provide a temperature distribution similar to that created using nuclear heating. Detailed information on the use of electrical heaters to simulate nuclear heating can be found in El-Genk and Xue, 1994.

The interelectrode gap between the emitter and collector is filled with cesium vapor during normal operation. The cesium is supplied by a single liquid cesium reservoir that is heated by one of the NaK coolant return lines. The cesium in the gap is constantly vented to space at a rate of approximately 0.5 g/day. This is one of the limiting factors in the reactor lifetime. (Schmidt et al., 1994) During normal operation, the cesium pressure in the gap is maintained around 1.5-2.0 torr (Paramonov and El-Genk, 1994).

Axial and radial temperature distributions in the reactor core cause performance differences in the 37 TFEs. The exact performance characteristic of each individual TFE is difficult to determine due to the following: (1) the thermal coupling of each TFE with the TFEs surrounding it, or lack of TFEs; (2) the electrical coupling of each TFE with the other TFEs, either in series for the 34 load power producing TFEs or in parallel for the 3 pump power producing TFEs; (3) all TFEs share a common heat removal system; and (4) all TFEs share a common cesium system. To understand the individual thermionic performance of a TFE, the TOPAZ-II TFE test stand must be used. This test stand allows detailed analysis of a single TFE under unique operating characteristics.

IV. TEST STAND DESCRIPTION

The TOPAZ-II TFE test stand is used to perform non-nuclear testing of a single TOPAZ-II TFE. This allows the TFE performance to be determined without the interference of the rest of the TOPAZ-II reactor systems and without any interfering effects caused by the TFEs relative location in the core (see Figure 3-2). Interference by the reactor systems include the direct thermal coupling of the TFE to the NaK coolant, coolant pump, and radiator, and the electrical coupling of the TFE to the other TFEs connected in series in the reactor core. The test stand also allows varying certain parameters which could not be varied on the entire reactor system to investigate their effect on TFE performance. These parameters include varying cesium vapor pressure in the interelectrode gap, the removal of all cesium vapor from the interelectrode gap, changing the collector sleeve temperature (directly effecting the collectors temperature), and operating the TFE at its operational limits to determine break-down characteristics.

The test stand contains the test apparatus within a vacuum chamber along with the associated vacuum, cesium, helium, and cooling water systems external to the vacuum chamber. As with almost all Russian structural components, the vacuum chamber is constructed mainly of Russian stainless steel type 12X18H10T. Phillips Laboratory has determined that this type of Russian stainless steel is closely approximated by the American Iron and Steel Institute (AISI) standard 321. The vacuum system is used to initially evacuate the vacuum chamber, the helium cavities, the cesium vapor system, and the TISA heater channel. The test stand start-up procedure requires an involved evacuation and out-gassing procedure. Out-gassing is performed by numerous heaters throughout the test stand.

The cesium system is used to supply cesium vapor to the interelectrode gap and to maintain the cesium vapor pressure. The system also provides a means to purify the cesium inventory. When the test stand is operating, cesium vapor is provided to the interelectrode gap by a cesium reservoir that is inside the vacuum chamber. This isolates the internal cesium system from the rest of the system outside of the vacuum chamber. Cesium vapor pressure in the interelectrode gap is regulated and varied by adjusting the inner cesium reservoir saturation temperature. An external cesium reservoir is provided to evacuate and fill the cesium system when the test stand is not in operation. (Luchau et al., 1993)

The helium system provides helium to the cavities and gaps inside the test stand, a means to purify the helium supply and a means to evacuated the helium from the system. Helium is used to fill in the gaps in the test apparatus to facilitate and control the heat transfer process. Collector sleeve temperatures can be controlled by varying the pressure in the regulate helium gap. The mechanism by which the thermal conductivity of helium is affected by pressure is discussed in detailed in the next chapter.

The water cooling system picks up the excess heat throughout the test stand. The components cooled by the water system include electric drives for various valves, vacuum pumps, cesium reservoirs, transistor load bank and the test apparatus. The volumetric flowrate of the cooling water flow to the test apparatus is measured using a turbine type flowmeter in the inlet line. The inlet and outlet cooling water temperature is measured by type-K, surface contact thermocouples on the inlet and outlet stainless steel piping. Two thermocouples are used on the outlet piping, one on the outlet pipe that is in thermal contact with the vacuum chamber and the other on the outlet pipe that is not in thermal contact with the vacuum chamber. The experimental data show that both of these temperature measurements are well within the thermocouple tolerance of each other. The

flowrate and temperature measurement accuracies are critical to the thermal modeling of the test stand.

The stand utilizes an automatic control system, an automated data acquisition system, and a variable electrical load bank. The entire control and data acquisition system was completely upgraded from the original Russian system to a United States technology based system. This upgrade occurred between the first set of tests in March of 1994 and the second set in August of 1994; however, the testing parameters were maintained the same during both data sets. The load bank is composed of both a transistive and a resistive load bank. The load bank can be controlled by a micro-computer to provide current-voltage (I-V) sweeps for the TFE. These sweeps are important in determining the actual operating characteristics of the TFE. (Luchau et al., 1993)

A diagram of the test apparatus is shown in Figure 4-1 (based on Luchau et al., 1993). The upper and lower helium chambers provide helium to the unregulated gaps in the test section and to the spaces in the TISA heater. The cesium for the inter-electrode gap enters the test section through the lower helium chamber which is heated during testing to prevent "cold-spots" in the cesium line. Since the lower helium chamber is heated and the upper helium chamber is not heated, heat losses out of the top and bottom of the test apparatus are different. This difference in the end losses will affect the test stand's thermal model. The upper and lower helium chambers also contain the electrical connections to both the emitter and collector. Electrical connections to the TISA heater are made in a chamber above the upper helium chamber.

A lengthwise cross-sectional view of the test stand's working section is shown in Figure 4-2. This figure shows the relative proportions of the various test section concentric cylinders. The overall length of the thermionic working section is 375.0 mm. The length of the TISA heater is 300.0 mm and the length of the cooling water jacket is
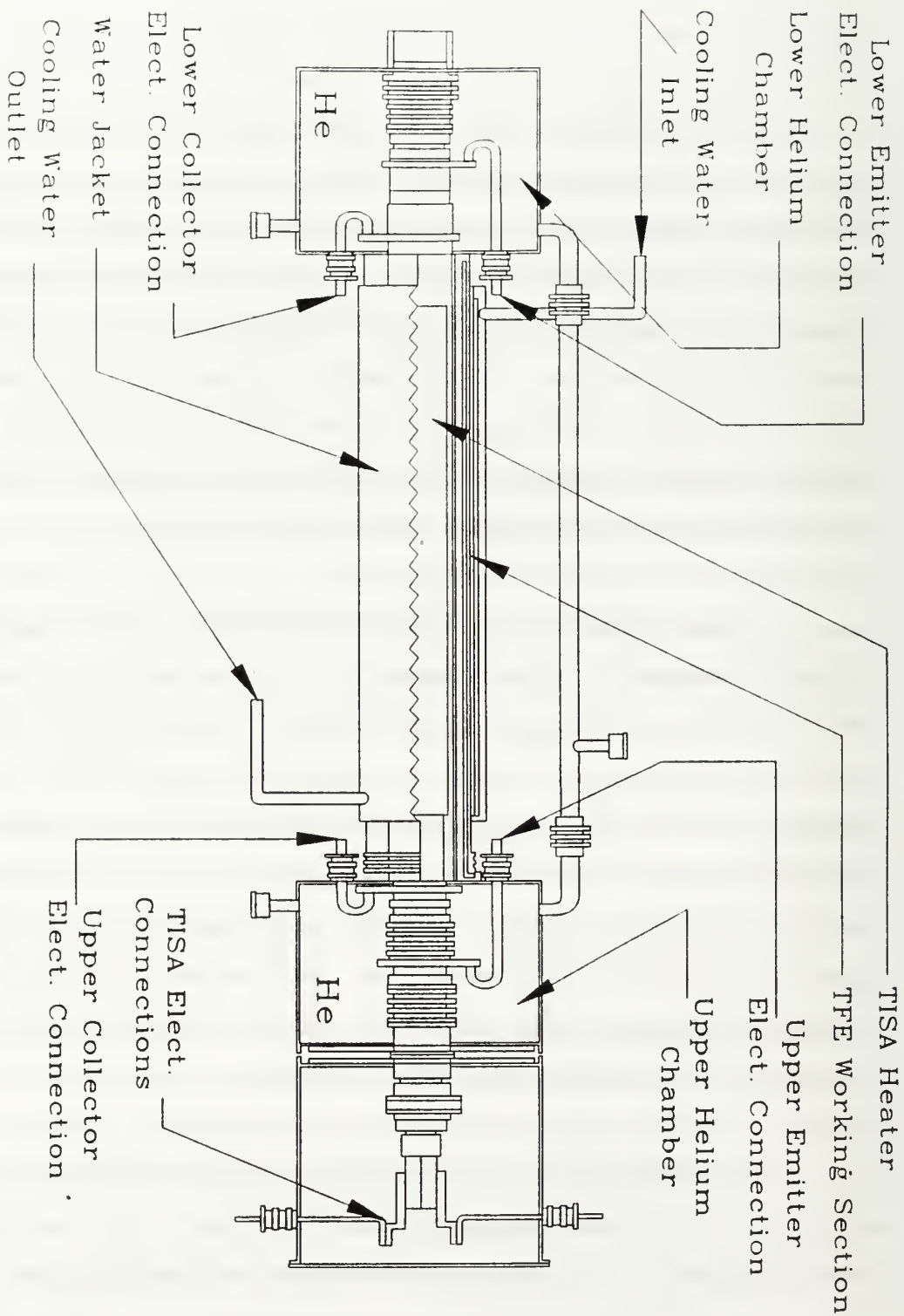
Figure 4-1. Cross-sectional View of the TOPAZ-II TFE Test Stand.

Lower Emitter
Elect. Connection

Lower Helium
Chamber

Cooling Water
Inlet

Lower Collector
Elect. Connection

Water Jacket

Cooling Water
Outlet

TISA Heater

TFE Working Section

Upper Emitter
Elect. Connection

Upper Helium
Chamber

TISA Elect.
Connections

Upper Collector
Elect. Connection

He

He
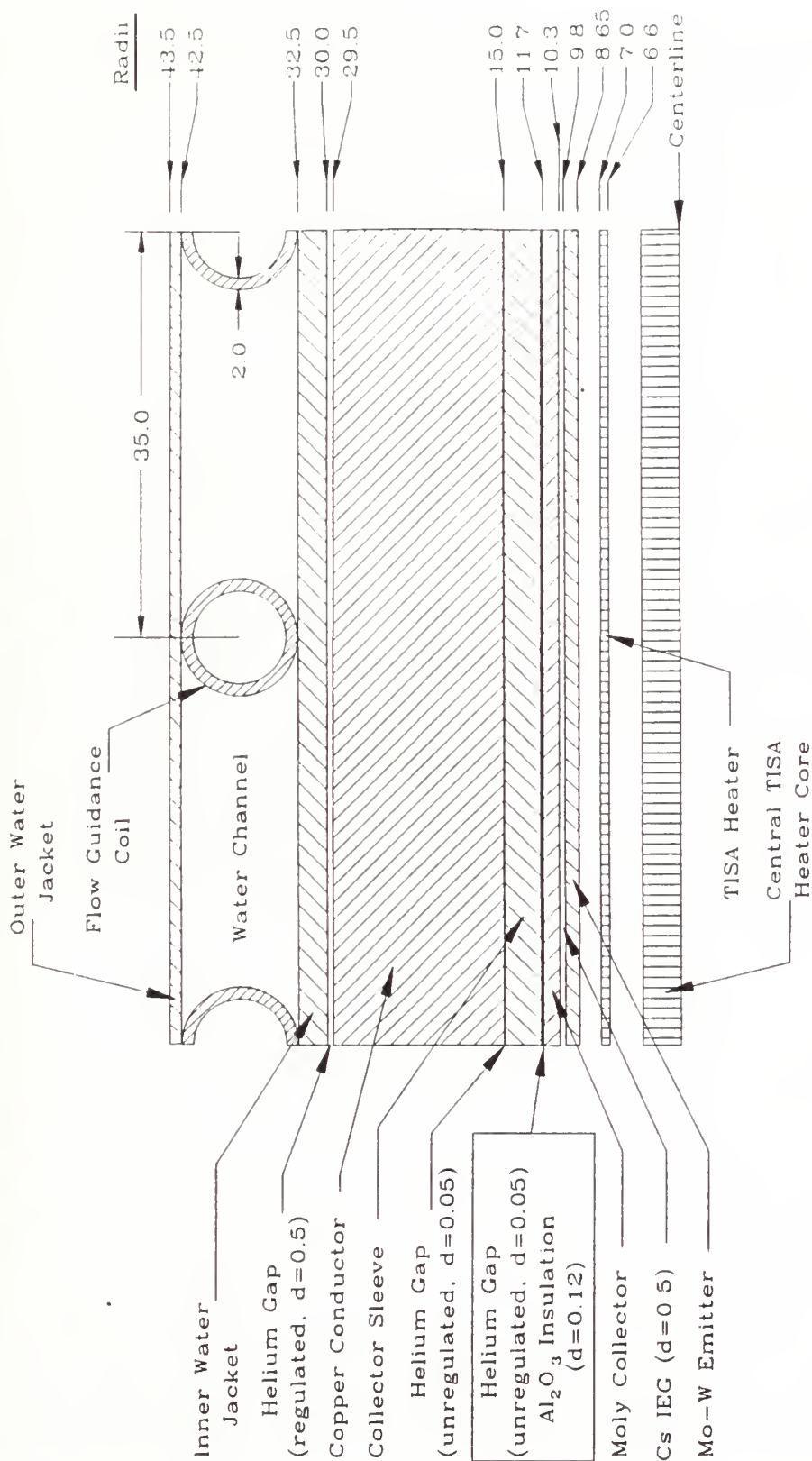
Figure 4-2. Cross-sectional View of a TOPAZ-II TFE in the Test Stand. (all deminsions in mm)

approximately 326.0 mm. The extremely small dimensions and close tolerances gives an indication of the difficulty associated with the manufacturing of the test section. A radial cut-away view of the complete test stand is shown in Figure 4-3. An enlarged view of the portion of the test stand from the collector sleeve inward is shown in Figure 4-4. The overall diameter of the entire test section is only 87.0 mm giving an L/D of 4.31 for the working section.

The TFE and its associated TISA heater are fit into the collector sleeve tube of the test stand as shown in Figure 4-4. The TISA heater is constructed of a special tungsten heating element and flexible lobes that act as thermocompensators. The maximum supply voltage is 29 VAC with a maximum current of 170 A. The TISA heater can supply a maximum heating power to the working section of 4500 W (Wold et al., 1993). The inner conductor of the TISA heater has a diameter of 6.5 mm and the outer conductor has a thickness of 0.4 mm and an outer diameter of 7.0 mm. The length of the heater is 300.0 mm which makes the heater 37.5 mm shorter at each end than the actual thermionic working section. This shorter length simulates the end effects associated with nuclear heating. Detailed discussions of the correspondance of TISA heating to nuclear fuel heating are presented in El-Genk and Xue (1993).

The thermionic device consists of concentric emitter and collector cylinders separated by an interelectrode gap and is 375.0 mm in length. The emitter cylinder is 1.15 mm thick with an outer diameter of 19.6 mm. The emitter is made of a monocrystalline molybdenum - 3% niobium alloy with its exterior surface coated with a 0.1 mm thick monocrystalline tungsten layer. The 0.5 mm interelectrode gap is filled with cesium vapor during normal operation. The interelectrode gap is maintained by the use of scandium-oxide (Sc_2O_3) spacers which prevent shorting between the emitter and collector. A total of six spacer sets are located axially along the TFE working section. These spacers are not shown in any of the figures. The collector cylinder is 1.4 mm thick with an

Radii (mm)	
43.5	Outer Water Jacket
42.5	Water Channel
32.5	Inner Water Jacket
30.0	Helium Gap (regulated)
29.5	Copper Conductor
15.0	Helium Gap (unregulated)
	Collector Sleeve
	Helium Gap (unregulated)
	Al_2O_3 Insulation
	NiCr Heating Elements
	TISA Heater Core
	TISA Heater
	Moly Collector
	Cs IEG
	Mo–W Emitter
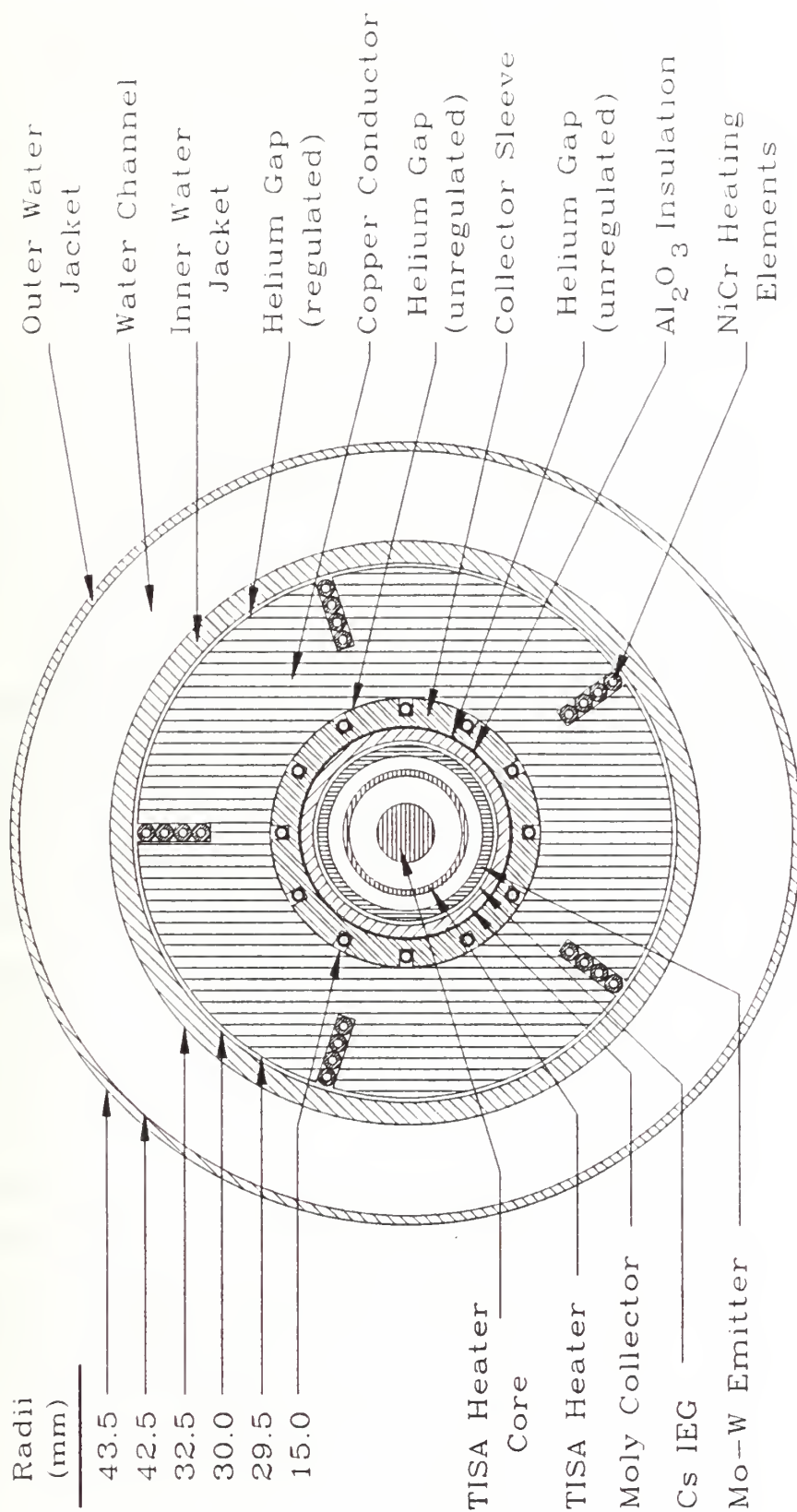
Figure 4-3. Radial Cut-away View of a TOPAZ-II TFE in the Test Stand.

Radii
(mm)

15.0 ——————————————— Stainless Steel
                                    Tube
11.7 ————————————————————
10.3 ————————————————— Thermocouple
9.8 ———————————————— Collector Sleeve
8.65 ——————————————— Helium Gap
7.0 ——————————————— (unregulated)
6.6 ——————————————— Al₂O₃ Insulation
3.25 —————————————— Moly Collector

TISA Heater ————————————— Cs IEG

TISA Heater ————————————— Mo–W Emitter
  Core
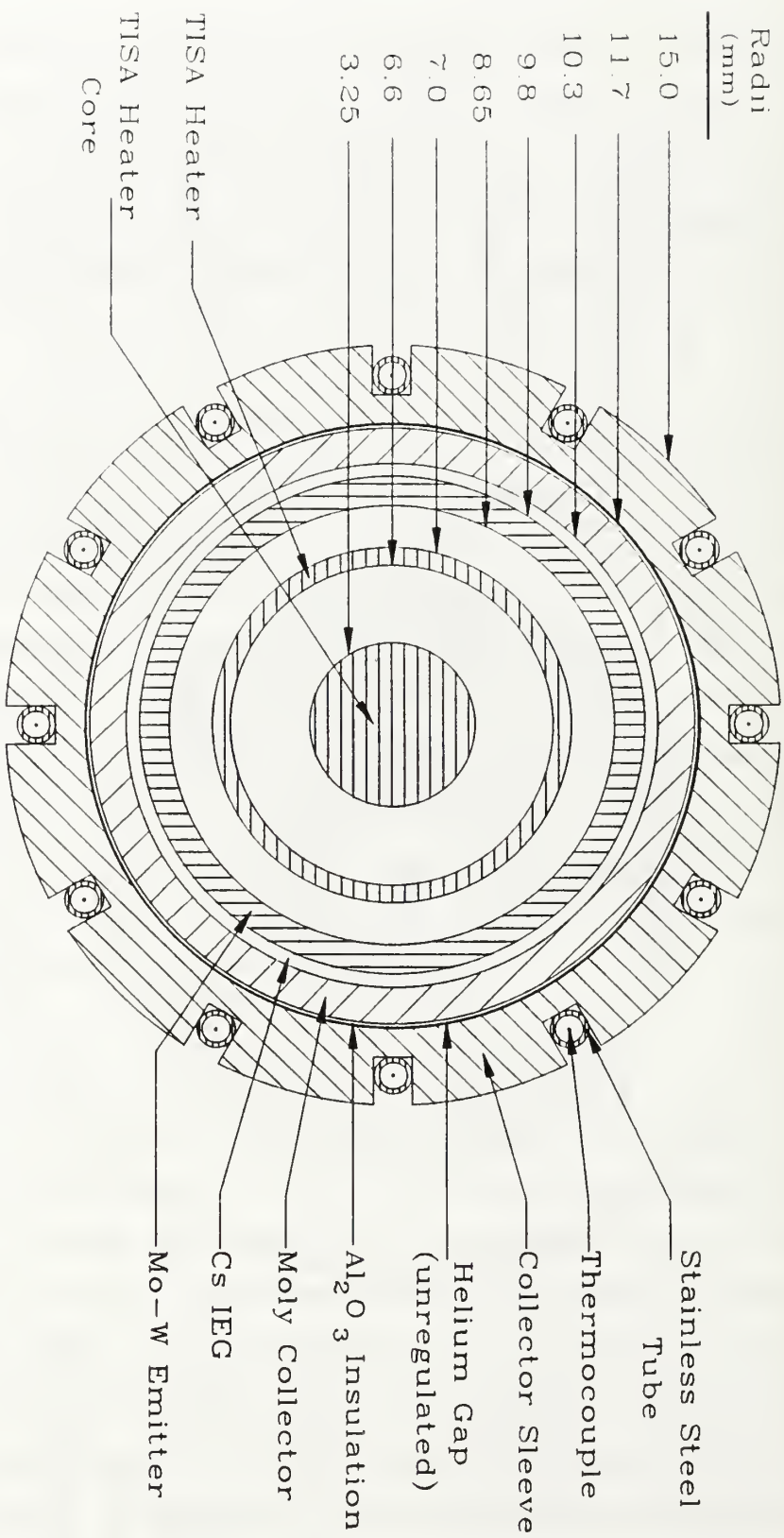
Figure 4-4. Radial Cut-away Detail of a TOPAZ-II TFE in the Test Stand.

24

inner diameter of 20.6 mm. The collector is made of polycrystalline molybdenum with its outer surface coated by a 0.15 mm layer of alumina (Al_2O_3). The alumina electrically insulates the TFE from the remainder of the test rig. The thermionic device and TISA heater used in the test stand are identical in construction to that used in the actual TOPAZ-II reactor.

A 0.05 mm gap separates the alumina insulator from the collector sleeve tube. This gap allows the TFE to be fit into the test rig and is filled with helium during normal operation. The helium is provided by the upper and lower helium chambers (see Figure 4-1). The helium pressure in this gap is unregulated and is normally in the 200 to 300 torr range.

The collector sleeve tube is 3.0 mm thick with an outer diameter of 29.9 mm. It is constructed of Russian 1X18H10T stainless steel. The collector sleeve contains 12 evenly spaced, 2.0 mm deep slots in its outer surface that run the length of the collector sleeve. Figure 4-5 shows the relative location of the thermocouple slots in the collector sleeve. These slots contain the only thermocouples located in the interior of the test rig. The thermocouples are positioned along the collector sleeve to provide an axial temperature distribution in the working section. The thermocouple wires are packed in alumina inside of stainless steel tubes which are laid inside the slots. These thermocouples are positioned in the test rig at the location where the NaK liquid metal cooling flows through the TFE in the actual TOPAZ-II reactor. This allows correlation of the test stand data to data obtained from the complete reactor testing. Another 0.05 mm helium gap separates the collector sleeve tube from the copper conductor. This small gap is for assembly purposes only. The helium in this gap is also supplied from the upper and lower helium chambers and is unregulated in pressure.

25
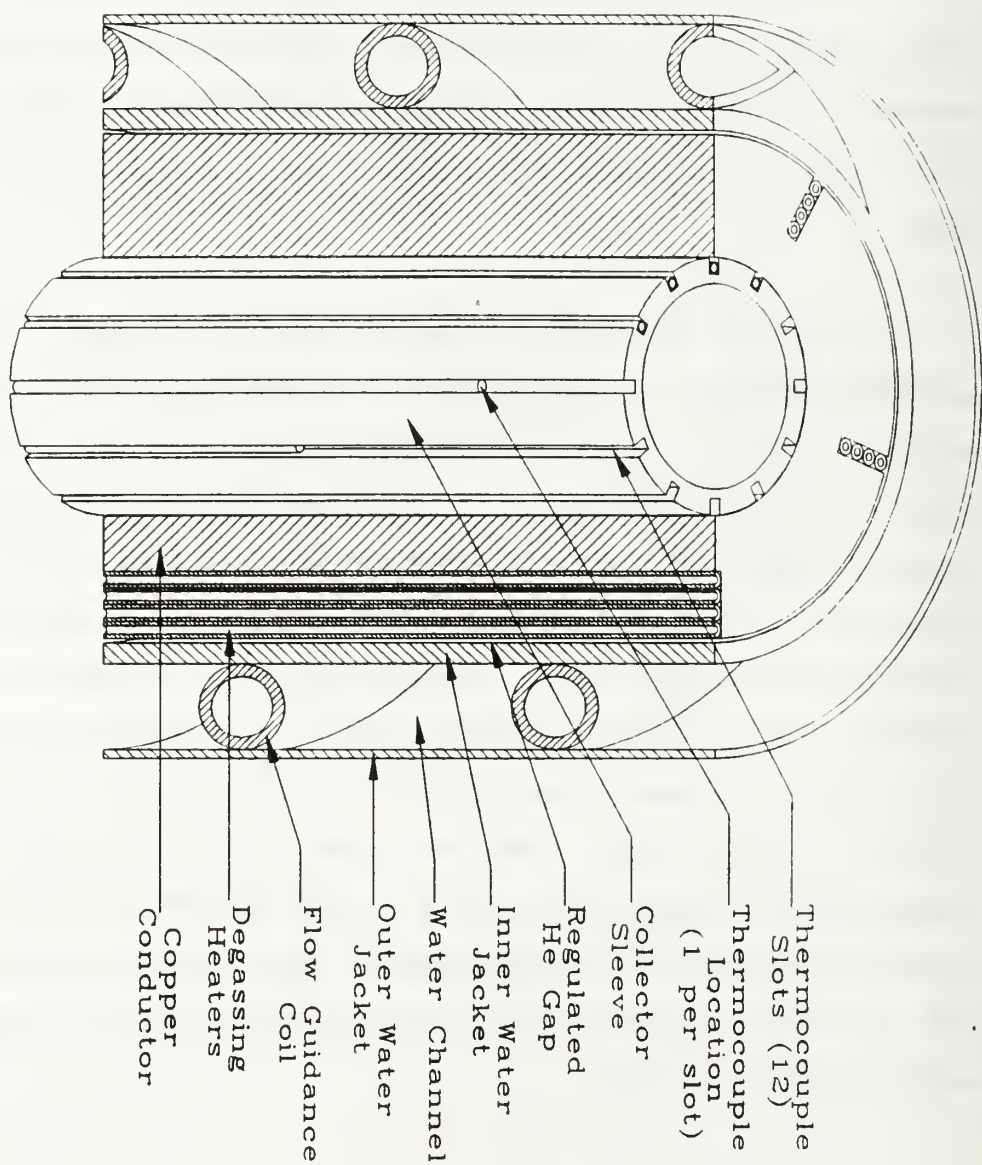
Figure 4-5. Thermocouple Slot Location in the Collector Sleeve.

Thermocouple
Slots (12)

Thermocouple
Location
(1 per slot)

Collector
Sleeve

Regulated
He Gap

Inner Water
Jacket

Water Channel

Outer Water
Jacket

Flow Guidance
Coil

Degassing
Heaters

Copper
Conductor

The copper conductor is 15.0 mm thick with an outside diameter of 60.0 mm. It is made of 99.99% pure copper and provides a heat transfer medium outward to the cooling water. The outer surface contains five radially spaced slots that each contain four nichrome (NiCr) heating elements. These heaters are used for outgassing the rig prior to startup and are secured during normal operation. The heater wires are insulated with alumina and sheathed in stainless steel. A 0.5 mm gap separates the copper conductor from the inner cooling water jacket. This gap is filled with helium supplied from a source external to the test rig. The pressure of the helium is regulated in the band of 1 to 10 torr during normal operation to control the collector sleeve temperature by varying the thermal resistance of the gap. The exact mechanism through which the helium thermal conductivity is affected by helium pressure is discussed later in the thesis.

The cooling water jacket is made of Russian 1X18H10T stainless steel and has an inner wall thickness of 2.5 mm and an outer wall thickness of 1 mm. A coiled stainless steel tube between the jacket walls provides a spiral flow path for the cooling water. The water flows from the bottom to the top of the water jacket around the outside of the coil in the cooling "channel" depicted in Figure 4-2. The coils are spaced by 35.0 mm and spiral approximately 6.5 times from bottom to top. Cooling water temperature is measured on the inlet and outlet piping exterior to the vacuum chamber using surface thermocouples. Cooling water flow rate is measured in the inlet piping using a turbine-type flowmeter located exterior to the vacuum chamber.

V. TEST STAND THERMAL ANALYSIS

As discussed in Chapter III, the thermionic cycle is a relatively inefficient conversion process. The TOPAZ-II TFE has a maximum efficiency of 5-6%; therefore, at least 94% of the heat generated by the TISA heater must be dissipated as a loss. Detailed thermal analysis of the test stand can provide a better understanding of how testing a single TFE in the test stand correlates to operating a TFE in the TOPAZ-II reactor core. The developed thermal model also yields valuable information about the limitations of the test stand for future testing and the validity of past and future test results.

A.   THERMAL MODEL INPUTS

The amount of input power to the test stand is determined by measuring the input current to the TISA heater through an external shunt and by measuring the voltage drop across the input terminals of the TISA heater. Multiplying the current in amps by the voltage in volts gives the input power to the TISA heater in watts and is designated as P_{TISA}. This TISA input power must be corrected to calculate the amount of power actually delivered to the emitter of the TFE. Correction is required to take into account the lead and line losses associated with the heater. Although Russian documentation for calculating the correction factor was not available, the Russian technicians at TIP use a correction factor of 88%. Correcting the input power to the TISA heater by this factor provides the amount of actual power delivered to the "active zone" of the TFE. This active zone power is designated as P_{az}.

The output power produced by the TFE is determined by measuring the current through the external load bank and by measuring the voltage drop across the upper and lower emitter or collector terminal connections (see Figure 4-1). Since the voltage drop is

29

measured directly across the interior terminal connections of either the emitter or collector, no correction factor is required to determine the output voltage of the TFE. Multiplying the voltage in volts by the current in amps gives the TFE output power in watts and is designated as P_{out}.

The only temperatures that are actually measured internally in the test stand are the collector sleeve temperatures. These measurements occur 1.8 mm into the stainless steel collector sleeve from its inner cylindrical surface (see Figure 4-4). As discussed in Chapter IV, the thermocouples in the collector sleeve provide axial temperature measurements along the length of the working section. There are a total of 12 thermocouples in the collector sleeve which are designated T56 through T67. During the data collection runs, thermocouple T64 was inoperative and was disregarded in the analysis. Thermocouples T59 and T60 and thermocouples T61 and T62 measure the temperature at the same location along the collector sleeve. Relative locations of the thermocouples with respect to the centerline of the working section are shown in Figure 5-1. The lengths of the TISA heater, the thermionic working section, and the water jacket and the approximate locations of the cooling water inlet and outlet are also shown in Figure 5-1.

In a one-dimensional model, it is necessary to take an average of the 11 operating collector sleeve thermocouples to obtain a value to use as an input temperature. Although many variables effect the magnitude of the collector sleeve axial temperature profile, the profile shape is generally the same under all conditions. Figure 5-2 shows a typical axial temperature profile at a TISA heater input power of 2400 W. The temperature data points are shown as diamonds with T56 at the -205 mm position and T67 at the 205 mm position. The dashed line represents a third-order polynomial curve fit of the data.
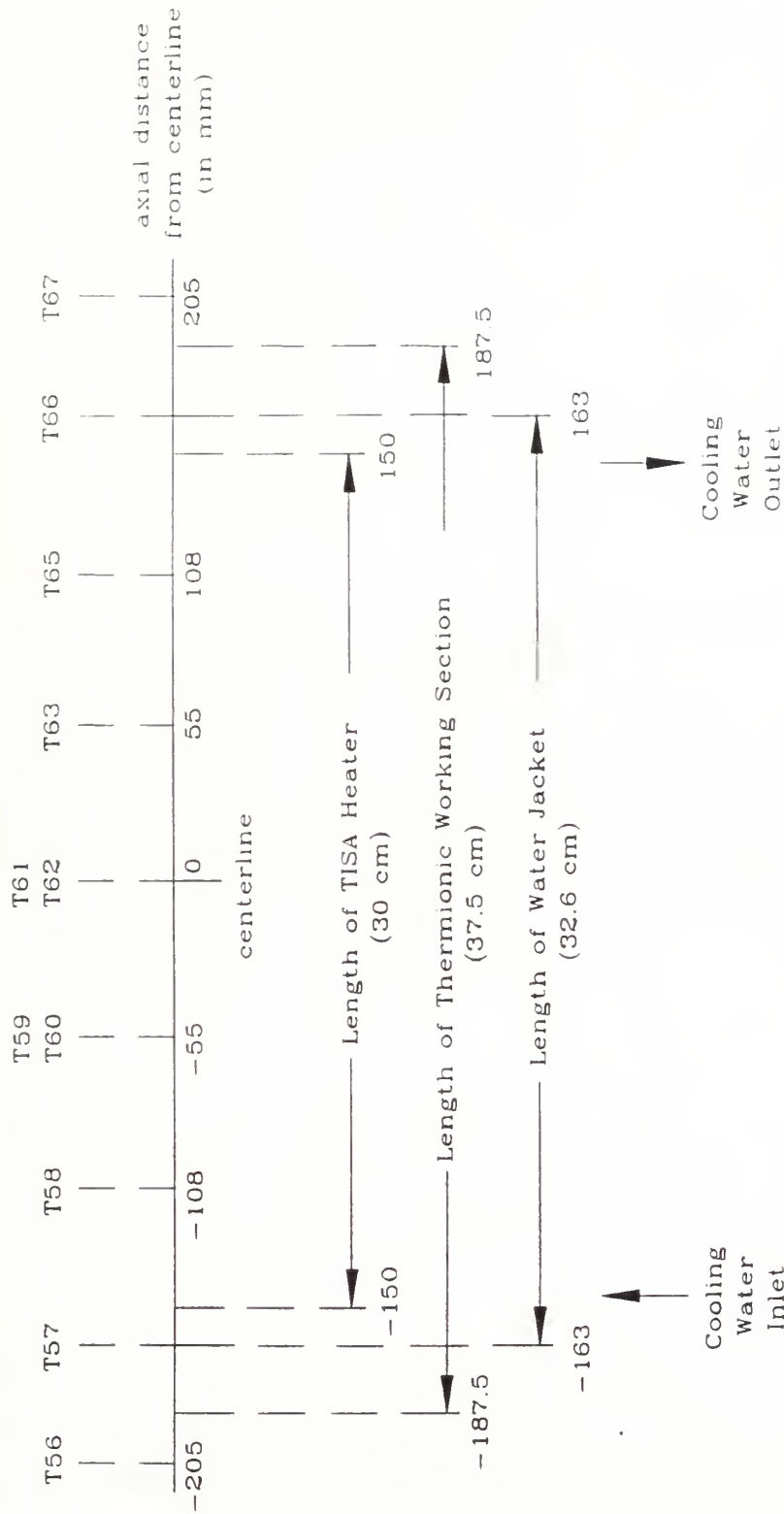
Figure 5-1. Axial Location of the Collector Sleeve Thermocouples.
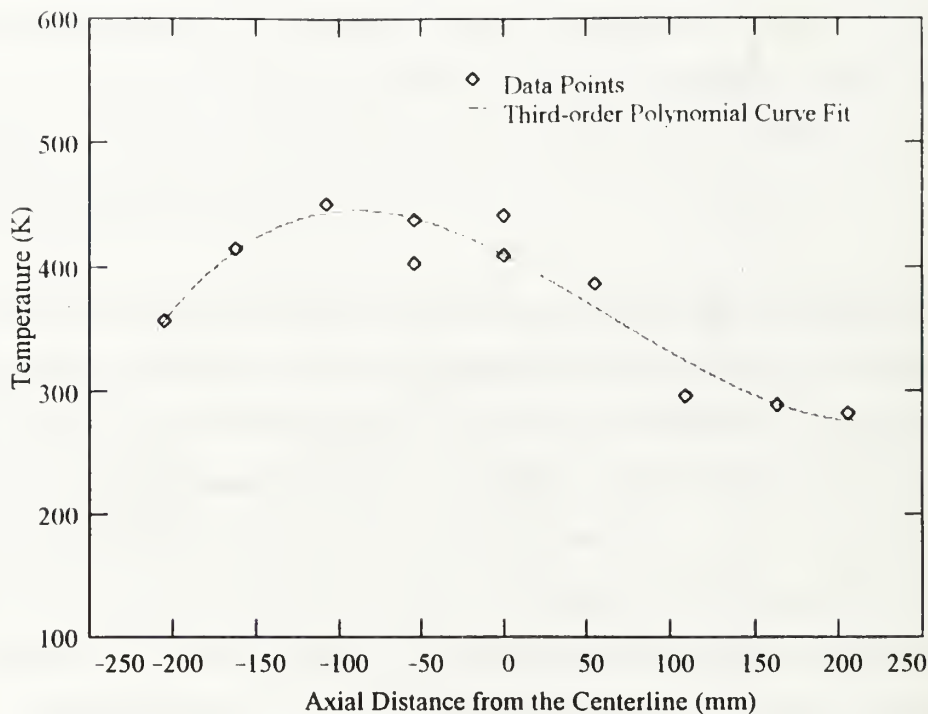
Figure 5-2. Typical Axial Temperature Distribution along the Collector Sleeve.

Although the TISA heater provides a fairly uniform temperature profile into the emitter, several reasons inherent to the test stand design cause the distribution to take the shape as shown in Figure 5-2. An overall downward slope in the data is expected due to the cooling water flowing from the bottom to the top of the working section; however the end effects of the upper and lower helium chambers cause the data to not be linear at the two ends of the graph. A straight average of the 11 data points would bias the temperature input to the thermal model low due mainly to the end effects. This biasing can be minimized if the end data points (T56 and T67) are not used and an average is taken only of the remaining nine data points. For example, the average of the 11 data points in Figure 5-2 is 379.0 K. Excluding the end data points gives an average of 392.1 K which is approximately 3.5% higher. For all calculations performed in this analysis, the average collector sleeve temperature was determined by excluding T56 and T67. A much more detailed two-dimensional model would be required to understand the error associated with this approximation.

32

The cooling water system provides the last of the measured test stand quantities necessary for the thermal analysis. Instrumentation of the cooling water system was required in support of this thesis since the information on the cooling water system was not previously deemed necessary. Surface thermocouples were placed on the cooling water inlet and outlet lines, exterior to the vacuum chamber. Approximately one meter of piping separates the actual thermocouple location from the inlet and outlet piping penetrations on the test stand. No corrected factor was used on these temperature measurements for any potential piping losses between the test section and the exterior of the vacuum chamber because the only method of heat transfer from the water piping would be by radiation heat transfer to the interior of the vacuum chamber. Since the maximum water temperature inside the piping is less than 40 °C over all the data runs, radiation heat transfer is not significant. The water piping is also in thermal contact with the vacuum chamber which provides another potential heat loss by conduction heat transfer to the vacuum chamber itself. Some uncertainty could have been removed if the thermocouples had been placed on the piping inside the vacuum chamber at the entrance and exit of the test section. This was not done for any of the data runs used in this analysis due to time constraints and the complexity of removing the vacuum chamber. An average bulk water temperature in the water jacket can be estimated by taking an average of the inlet and outlet water temperatures.

A turbine-type flow meter was also installed on the inlet cooling water line prior to the data runs. The accuracy of the flow meter was physically verified to be within 2% of the indicated flow rate over the range used during the data runs. Initially the data runs were taken with the cooling water isolation values fully open which was the normal operating procedures for the test stand. However, with the valves fully open, the change in cooling water temperature between the inlet and the outlet was less than 5 °C. Since the accuracy of the surface thermocouples is only ± 1 °C, a larger temperature change is desired to reduce the percent error. Around halfway through the first set of data runs, the flow rate was throttled down to approximately 0.7 gpm. This gave a temperature change

between 10 to 15 °C over most of the data runs. All of the data collected during the second set of data runs were collected at a flow rate of approximately 0.7 gpm.

B.   THERMAL MODEL

Difficulty was encountered during the thermal analysis of the test stand due to the small number of input parameters and the large number of "unknowns." In order to better understand the scope of the problem, a thermal analysis flowchart was developed. Figure 5-3 shows the test stand thermal analysis flowchart. Data collected from the test stand are shown as circle and are used as inputs into the thermal model. From this flowchart it can be seen that the problem divides itself into the following three sections: (1) thermal network calculations; (2) water channel heat removal calculations; and (3) coupling the thermal network calculations with the TOPAZ-II Thermionic Transient Analysis Model (TITAM). TITAM is a computer model developed by the University of New Mexico to simulate the operation of the entire TOPAZ-II reactor system under steady-state and transient conditions (Paramonov and El-Genk, 1994). The basis for the entire analysis is the thermal network.

1. Thermal Network

The one-dimensional losses through the test stand are modeled using a network method. Figure 5-4 shows a simplified representation of the resistance network used for thermal modeling the test stand. The network starts at the outside wall of the cylindrical emitter and runs outward to the centerline of the water channel. The three major modes of heat transfer encountered throughout the network are radiation, conduction, and forced convection. Radiation heat transfer was considered a heat transfer mode through all of the test stand gaps when the thermal network was initially developed. It is shown later in this section that radiation heat transfer plays an insignificant role in the heat transferred

34

Figure 5-3. Test Stand Thermal Analysis Flowchart.

35

Figure 5-4. Thermal Model Resistance Network.

36

through the unregulated and regulated helium gaps; however, radiation heat transfer does play an important role in the cesium interelectrode gap. Conduction heat transfer occurs through all of the metal components and through the gaps in the test stand; including the cesium interelectrode gap, the two unregulated helium gaps, and the regulated helium gap. Forced convection occurs into the cooling water flowing through the water channel.

The basic heat transfer equation used for conduction heat transfer through a cylindrical wall is found in Wong (1977). Equation 5.1 gives the equation used for the metal components of the test stand:

$$Q = \frac{1}{R_c} (T_{hot} - T_{cold}) \tag{5.1}$$

where: R_c = thermal resistance (K/W)
T_{hot} = hot wall temperature (K)
T_{cold} = cold wall temperature (K)

The thermal resistance, R_c, is calculated for hollow cylinders using Equation 5.2:

$$R_c = \frac{\ln(\frac{r_o}{r_i})}{2\pi z k} \tag{5.2}$$

where: r_o = outer wall radius (m)
r_i = inner wall radius (m)
z = cylinder length (m)
k = material thermal conductivity (W/mK)

For the test stand, T_{hot} will be the temperature at the inner cylindrical surface and T_{cold} will be the temperature at the outer cylindrical surface of the component of interest. For the thermal model calculations, the temperature subscript will indicate the node at which the temperature is measured.

A cylindrical length of 30.0 cm is used in all of the calculations. This length corresponds to the total length of the TISA heater; however, as can be seen in Figure 5-1, the length of the TISA heater, the length of the water jacket, and the length of the TFE working section are all different. Since there is a 20% increase in cylinder length from the TISA heater length to the TFE working section length, the thermal resistance also increases by 20%. Although this only results in a few degree Kelvin difference in the ΔT across a single metal component, the cumulative effect of this difference can lead to large calculational uncertainty. The shortest of the possible cylinder lengths is used in the analysis since it gives a more conservative result.

The thermal conductivities of all the different test stand components are graphed as a function of temperature in Appendix A. Since the thermal conductivity is a function of temperature and the metal components have a decreasing temperature distribution from the inner wall to the outer wall, an estimate of the thermal conductivity for the entire thickness must be made. When entering the thermal model, only one temperature is known; therefore, it is not possible to determine the average temperature of the component. For the first iteration through the network, the thermal conductivity of the component is calculated based on the one known temperature. Because metal is a very good conductor of heat, the thermal conductivity is fairly constant over the small ΔT effective across the metal. Based on calculations, using the one known temperature to estimate the thermal conductivity results in only a 0.4% difference than if the thermal conductivity were recalculated with the lower temperature found after calculating the ΔT. Therefore, less than a three degree Kelvin error is induced into the network and this makes recalculation of the thermal conductivity unnecessary.

The basic equation used for heat transfer for the gas filled gaps is found in El-Genk et al. (1993). This equation accounts for both radiation and conduction heat transfer through the gap and is given in Equation 5.3:

$$Q = \frac{1}{R_{r/c}} (T_{hot} - T_{cold} \qquad (5.3)$$

where: $R_{r/c}$ = radiation/conduction thermal resistance (K/W)

The radiation/conduction thermal resistance, $R_{r/c}$, is calculated using Equation 5.4:

$$R_{r/c} = \frac{\ln(\frac{r_o}{r_i})}{2\pi z(r_o - r_i)} \{ \frac{k_g}{d} + \sigma \varepsilon_{eff}(T_{hot}^2 + T_{cold}^2)(T_{hot} + T_{cold}) \}^{-1} \qquad (5.4)$$

where: k_g = gas thermal conductivity (W/mK)
$\quad$ d = gap width (m) = $(r_o - r_i)$
$\quad$ σ = Stefan-Boltzmann constant = 5.67×10^{-8} W/m²K⁴
$\quad$ ε_{eff} = effective emissivity

The thermal conductivity for helium as a function of temperature is graphed in Appendix A. According to Reid et al. (1977), the thermal conductivity of all gases can also be affected by the pressure in the gap, although for pressures greater than approximately 1 torr, the thermal conductivity only increases by about 1% for a pressure change of 760 torr. Therefore, for the unregulated helium gap pressures of 200-300 torr, the thermal conductivity is considered a function of temperature only. This estimation is valid because the mean free path for collisions between atoms is much less than the mean free path for collision between an atom and the walls; therefore, an atom does not have to travel far before transferring its energy to another atom and eventually reaching thermal energies. The pressure maintained in the regulated helium gap is around the lower end of where this approximation is considered valid. According to the experimental data collected, the thermal conductivity of helium in the 1-10 torr range is greatly affected by pressure. This unusual phenomenon is discussed in detail later in this chapter.

The effective emissivity can be calculated by assuming that the view factors from both surfaces are equal to 1, and the two surfaces areas are also equal by Equation 5.5 (Welty et al., 1984):

39

$$\varepsilon_{eff} = \cfrac{1}{\cfrac{1}{\varepsilon_i} + \cfrac{1}{\varepsilon_o} - 1} \tag{5.5}$$

where: ε_i = inner surface emissivity
ε_o = outer surface emissivity

Due to the extremely small dimensions and gap size, both of these assumptions are valid.

The basic equation used for forced convection heat transfer into the cooling water is found in Wong (1977). The equation used for calculating the heat transfer into the test stand cooling water is based on Newton's Law of Cooling and is given in Equation 5.6:

$$Q = \frac{1}{R_{fc}} (T_{wall} - T_{bulk}) \tag{5.6}$$

where: R_{fc} = forced convection thermal resistance (K/W)
T_{wall} = cooling water channel wall temperature (K)
T_{bulk} = bulk cooling water temperature (K)

The forced convection thermal resistance, R_{fc}, is calculated using Equation 5.7:

$$R_{fc} = \frac{\ln(\frac{r_o}{r_i})}{2\pi z (r_o - r_i) h} \tag{5.7}$$

where: h = convective heat transfer coefficient (W/m^{2}K)

The convective heat transfer coefficient is a complicated function of the cooling channel geometry, the thermophysical properties of the cooling water, and principally of the flow characteristics through the channel. This coefficient and the complexities encountered in its definition are discussed in detail later in this chapter.

An example of the data set used in the thermal network calculations is given in Table 5-1. These data are used in the following discussion to explain the thermal model calculational procedure. The data collected between 14-18 August, 1994, in support of this thesis are tabulated in Appendix B. The data presented in Table 5-1 were taken on August 17, 1994. As can be seen there, the TFE efficiency is less than 4%. This is mainly due to the interelectrode cesium pressure not being at its optimum value for an input power of 3000 W. At this power level, an interelectrode cesium pressure of approximately 1 torr would increase the TFE's efficiency closer to 5%. However, for thermal modeling purposes, optimum TFE performance is not important. Cesium optimization will be covered in detail in the companion thesis written by LT J. R. Venable that will be available after March of 1995.

P_{TISA} (W)	3,412	Minimum Collector Sleeve Temp. (C)	354.3
P_{az} (W)	3,003	Maximum Collector Sleeve Temp. (C)	515.6
P_{out} (W)	109	Average Collector Sleeve Temp. (C) T_6	453.7
Q_{loss} (W)	2,894	Cooling Water Flow rate (gpm)	0.69
Efficiency (%)	3.63	Cooling Water Mass Flow rate (kg/s)	0.04
Cs Pressure (torr)	0.5	Cooling Water Inlet Temp. (C)	16.6
Regulated He Gap Press (torr)	10	Cooling Water Outlet Temp. (C)	32.2/32.1

Table 5-1. Example Data Set for the Thermal Model.

Since the only temperature measured internally to the test stand is the collector sleeve temperature, the thermal network is entered at node T_6. From this node, calculations can be made to determine the temperature distribution either inward toward the center of the TFE or outward toward the water channel. In order to make these temperature calculations using basic heat transfer equations, the amount of heat transferred out through the test stand must be calculated. This transferred heat is equal to the portion of the TISA input power that is not converted to electricity in the TFE and is designated as Q_{loss}. Equation 5.8 shows the definition for Q_{loss}:

$$Q_{loss} = P_{az} - P_{out} \tag{5.8}$$

In a one-dimensional model for the test stand, Q_{loss} will travel only radially outward through the test stand components to be carried away by the cooling water flowing through the water jacket.

Using the node 6 temperature (T_6) and the amount of heat lost by the system (Q_{loss}) as a starting point, the thermal model is presented in two sections: (1) calculations from the collector sleeve to the water channel, and (2) calculations from the collector sleeve to the emitter. Detailed discussions about the critical resistances in the network are also be presented. The calculations made with the data from Table 5-1 are given in Appendix C.

a. From the Collector Sleeve to the Water Channel

The first resistance encountered in the thermal network is a 1.2 mm thick stainless steel collector sleeve. The thermal conductivity of the stainless steel is determined using Figure A-3. This thermal conductivity is then used to calculate the thermal resistance of the stainless steel using Equation 5.2. Using the calculated Q_{loss} as

42

the variable Q, Equation 5.1 can now be solved for T_{cold}, which corresponds to T_7, since all of the other equation variables have been defined.

A 0.05 mm unregulated helium gap is the next resistance in the thermal network. The thermal conductivity of this continuum helium gas (gap pressure of approximately 200 torr) is calculated using Figure A-4. The effective emissivity is then calculated using Equation 5.5. This equation requires the stainless steel emissivity which is found from Figure A-6 and the copper emissivity which is found from Figure A-7. Both of these emissivities are fairly constant over the temperature range of interest. Using Equation 5.4 in combination with Equation 5.3, the value for T_8 can be solved for numerically. If the contribution of the radiation heat transfer is ignored through the helium gap, and T_8 is solved for based on conduction heat transfer through the gap only, the answers for T_8 are the same within four significant digits. For this reason, radiation heat transfer through the unregulated and regulated helium gaps can be disregarded and the resistance network can be solved based on conduction heat transfer only.

The next resistance in the network is the copper conductor. Again Equations 5.2 and 5.1 are solved to determine the temperature on the outer cylindrical surface of the copper conductor, which corresponds to T_9. The regulated helium gap is the next resistance in the thermal network.

b. Regulated Helium Gap

As discussed earlier in this chapter, the pressure of the helium in the regulated gap is maintained between 1-10 torr, depending on the input power level, to hold the collector sleeve temperature fairly constant. Since the collector sleeve temperatures are measured at approximately the same radial location that the liquid metal cooling flows through the actual TOPAZ-II core, holding this temperature constant better

43

simulates the actual conditions in the core. The temperature at this radial position in the TOPAZ-II core is relatively constant due to the high heat capacity of the liquid metal cooling and the high heat rejection capability of the radiator.

Due to the low gap pressure, the helium is rarefied which indicates that the mean free path for collisions between atoms is much larger than the mean free path for atom to wall collisions. Paul Agnew of AEA Technology, United Kingdom, currently assigned to the TOPAZ-II Project and working in the area of materials science and thermionics, has completed a preliminary analysis on the pressure dependence of helium thermal conductivity at these low pressures. The initial results of his work indicated that helium thermal conductivity should approach its continuum value at a gap pressure of approximately 5 torr vice the 1 torr discussed in Reid et al. (1977). However, experimental results indicate that the helium thermal conductivity should be around 30% of its continuum value for a gap pressure of 10 torr. Detailed Monte Carlo computer programming and investigation of gas atom scattering mechanisms will be required to determine a more accurate model of the regulated gap. (Agnew, 1994)

Although a more exact solution is not possible without extensive work, the regulated gap helium thermal conductivity can be better approximated using the empirical data collected on the test stand. Since the regulated helium gap is separated from the cooling water channel by only 2.0 mm of stainless steel, the temperature of the inner wall of the cooling channel is directly dependent on the regulated helium gap thermal conductivity. Using the helium continuum thermal conductivity value calculated to be 0.276 W/mK for this example, gives a cooling channel inner wall temperature of around 325 °C. The cooling water is pressurized on average to a pressure not greater than 70 psig. Since the cooling system provides water to many different components, the actual pressure is dependent on the cooling system load conditions. This cooling water pressure gives a initiation boiling point temperature of approximately 140 °C. The wall temperature

44

calculated using the helium continuum thermal conductivity is around 185 °C greater than this boiling point temperature. Based on an cooling water outlet temperature of 32 °C, it is assumed that the water does not boil in the cooling channel. Figure 5-5 shows a graph of the cooling water channel inner wall temperature dependence on the regulated helium gap thermal conductivity. If the wall temperature is bracketed around 80 ± 30 °C, the regulated helium gap thermal conductivity ranges between 0.073-0.087 W/mK. This range is around 30% of the calculated continuum value.

This calculated range of helium gap thermal conductivities can be used along with Equation 5.1 to calculated a range of node 10 temperatures. Using these node 10 temperatures, the 2.0 mm thick stainless steel water jacket thermal conductivity can be determined using Figure A-3. The temperature at the inner wall of the cooling water
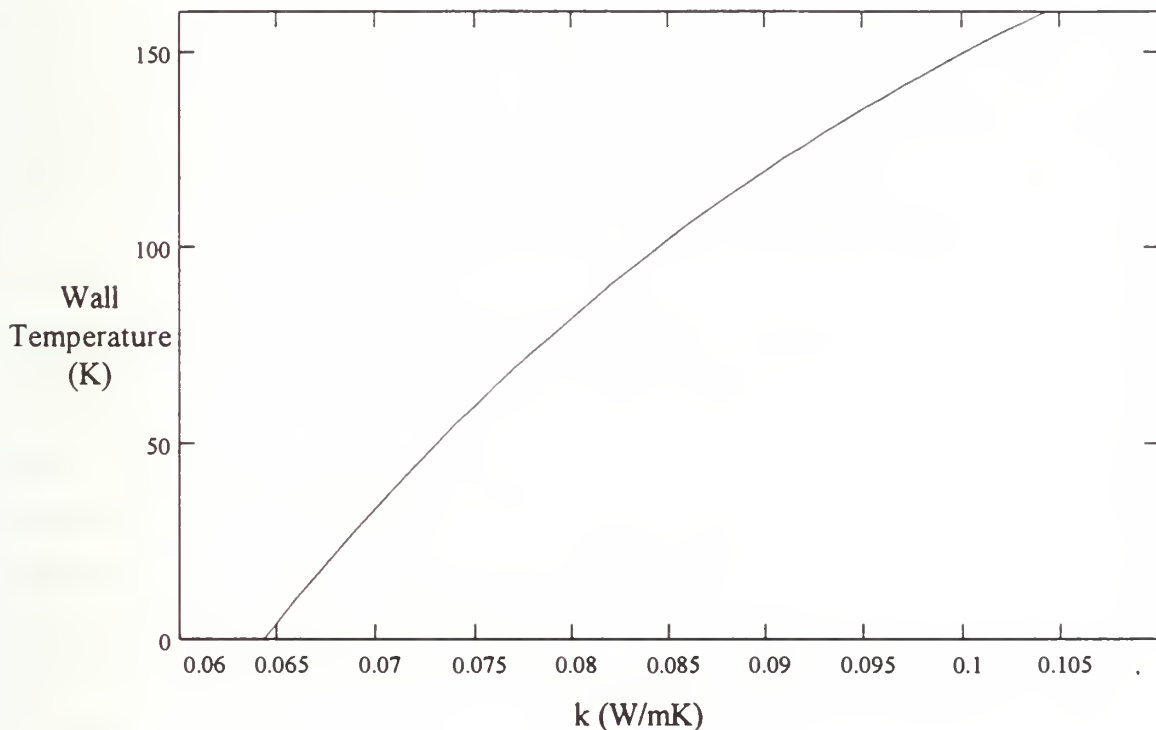
Figure 5-5. Cooling Water Channel Inner Wall Temperature Dependence on the Regulated Helium Gap Thermal Conductivity.

channel, corresponding to the node 11 temperature, is then calculated using Equations 5.2 and 5.1. These calculated wall temperatures range from 64-122 °C.

Using an estimated convective heat transfer coefficient and an estimated heat transfer area (the method used to estimate these parameters is discussed later in this chapter), the bulk water temperature can be estimated using Equations 5.7 and 5.6. These calculations yield a range of bulk water temperatures of 6-92 °C. Using an average of the measured inlet and outlet cooling water temperatures gives a bulk temperature of approximately 24 °C.

c. From the Collector Sleeve to the Emitter

The calculations for the inward portion of the thermal network are similar to the calculations made for the outward portion. The first resistance encountered is the inner portion of the stainless steel collector sleeve. The same thermal conductivity value is used for the collector sleeve as was used in the outward portion. Using Equations 5.2 and 5.1, the node 5 temperature can be found. This corresponds to T_5.

The next resistance in the network is another 0.05 mm unregulated helium gap. Radiation heat transfer is ignored and the heat transfer calculations using Equations 5.2 and 5.1 provide the temperature at node 4. Node 4 corresponds to the outer wall of the layer of alumina insulation on the collector. The thermal conductivity of alumina is found using Figure A-1 and the same conduction heat transfer calculations are completed to calculate the node 3 temperature, T_3. This temperature is the interface temperature between the collector and the alumina insulation.

The temperature at node 2, T_2, can be similarly calculated using the thermal conductivity of polycrystalline molybdenum found from Figure A-5. This

46

temperature corresponds to the inner surface of the collector and is an extremely important measurement to determine thermionic performance. The cesium interelectrode gap is the next resistance in the network.

d. Cesium Interelectrode Gap

The cesium interelctrode gap heat transfer mechanism is another critical resistance in the network that cannot be easily calculated with only basic heat transfer equations. Conduction and radiation heat transfer both play an important part in the overall heat transfer through the interelectrode gap. The thermal conductivity of the cesium in the gap depends on the gases vapor pressure, the emitter surface temperature, the collector surface temperature, and the gap size. (Paramonov and El-Genk, 1994)

Radiation heat transfer cannot be ignored through the interelectrode gap since the temperature of the emitter is high enough to make this mode of heat transfer significant (on the order of 1800 K). The effective emissivity for the gap cannot be calculated as presented for the helium gaps, but must be determined empirically. A detailed discussion on thermal modeling of the cesium interelectrode gap and coupling the thermal model with a thermionic emission model can be found in Paramonov and El-Genk (1994).

2. Water Channel Calculations

In order to calculate the thermal resistance using Equation 5.7, the convective heat transfer coefficient is required. Calculating the heat transfer coefficient for the water channel is complicated by the flow channel geometry and by the low water flow rates. Figure 5-6 shows the cooling water jacket details including the flow guidance coil. This flow guidance coil is a stainless steel tube with an outer diameter of 10.0 mm that fits

47
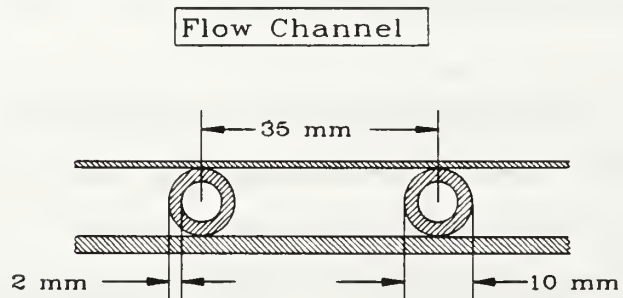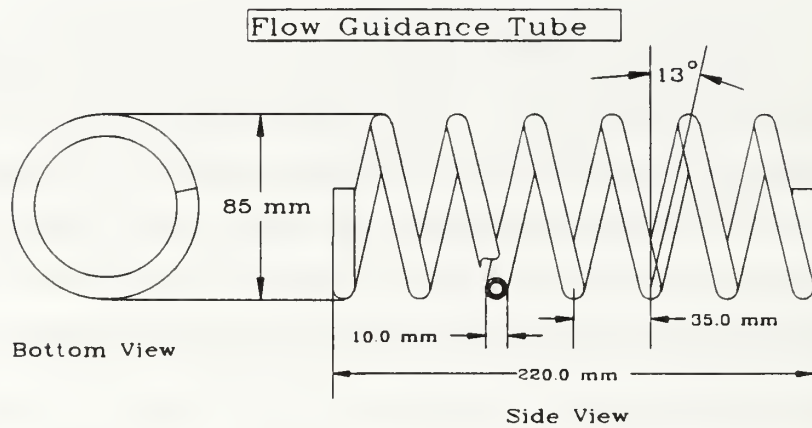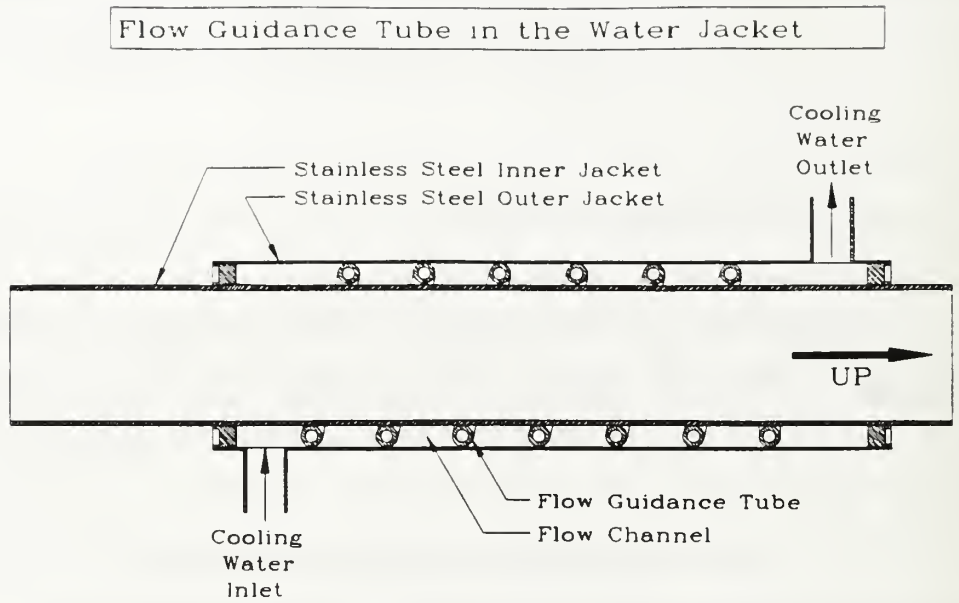
Figure 5-6. Cooling Water Jacket Details.

48

inside of the water jacket to direct the flow in a spiral path to facilitate forced convection heat transfer. The cooling water flows around the outside of the flow guidance coil with no flow through the coil itself.

As shown in Figure 5-6, the flow channel cross-sectional area is calculated by determining the cross-sectional area of a rectangle with dimensions of 35x10 mm, and subtracting off the cross-sectional area of the flow guidance coil (diameter of 10 mm). This gives a cross-sectional channel flow area of 2.7×10^{-4} m^2. The equivalent hydraulic diameter is calculated using the definition from Wong (1977), to be 0.011 m.

Following the definitions and equations presented by El-Genk and Rao (1986), the Reynolds number is calculated using this geometry and the given example flow rate to be 1480. This Reynolds number indicates that the flow falls into the combined laminar flow regime. The convective heat transfer coefficient can be defined from El-Genk and Rao (1986) and is given in Equation 5.9:

$$h = \frac{Nu \, k}{D_e} \qquad (5.9)$$

where: Nu = Nusselt number
k = water thermal conductivity (W/mK)
D_e = equivalent diameter (m)

In the combined laminar regime, the Nusselt number is dependent on the thermophysical properties (defined by the Graetz number) and the buoyant forces (defined by the Rayleigh number). This flow regime is immensely difficult to analyze with existing correlations.

Although the convective heat transfer coefficient cannot be determined exactly, several existing forced convection correlations can provide a range of possible coefficients. The upper limit is determined using the Dittus-Boelter correlation for fully

developed turbulent flow in a channel. This gives a convective heat transfer coefficient of 1012 W/m²K. The lower limit is found by the Seider-Tate correlation for developing laminar flow. This correlation gives a convective heat transfer coefficient of 528 W/m²K. Therefore, the actual coefficient will fall between the range of 528-1012 W/m²K and these limits can then be used in the resistance network to estimate the drop between the cooling channel wall temperature and the bulk water temperature.

Using the cooling water inlet and outlet temperatures along with the measured cooling water flow rate, the amount of heat carried away by the water can be calculated using Equation 5.10:

$$Q = \dot{m} \, c_p \, (T_{out} - T_{in}) \qquad (5.10)$$

where: $\dot{m}$ = cooling water mass flow rate (kg/s)
c_p = specific heat capacity of water
T_{out} = cooling water outlet temperature (K)
T_{in} = cooling water inlet temperature (K)

The heat carried away by the water, Q, should be equal to the heat lost by the TFE, Q_{loss}, if all of the excess heat traveled one-dimensionally out of the test section to be carried away by the cooling water. For the example data, the heat carried away by the cooling water is approximately 2840 W. This is less than 2% different from the 2894 W lost by the TFE. As can be seen from the experimental data presented in Appendix B, most of the data collected for the heat removed by the cooling water falls within 10% of the heat lost by the TFE. The percent error tends to increase as the input power level decreases. This is an expected result since the difference between the inlet and outlet cooling water temperature decreases as the power level decreases causing an increase in the expected error.

By setting Equation 5.10 equal to Equation 5.6, the convective heat transfer coefficient can be calculated based on a heat transfer surface area. Once again difficulty arises in determining the exact heat transfer surface area. From Figure 5-6 it can be seen that even though no cooling water flows through the flow guidance coil, the stainless steel coil is in thermal contact with the stainless steel water jacket. The maximum possible heat transfer surface area can be determined by summing the inner water jacket cylindrical surface area, the outer water jacket cylindrical surface area, and the total surface area of the flow guidance coil. The minimum possible heat transfer surface area is equal to the cylindrical surface area of the inner water jacket. These calculations are shown in Appendix D and give a range of heat transfer area between 0.067-0.203 m^2. Figure 5-7 shows a graph of the heat transfer coefficient plotted against the heat transfer area. Since
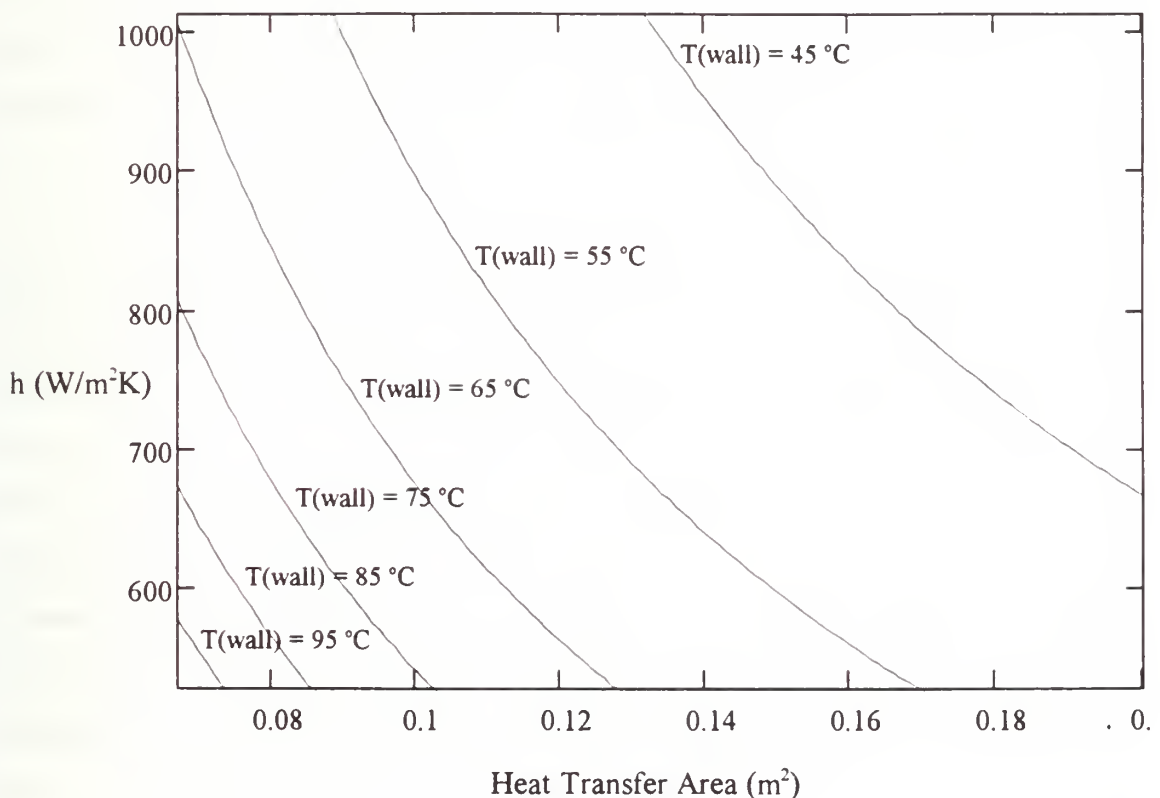
Figure 5-7. Cooling Water Heat Transfer Coefficient Dependence on the Heat Transfer Area.

the cooling water bulk temperature is known, the cooling channel wall temperature is varied from 45 °C to 95 °C. It can be seen from the figure that a wall temperature of greater than 95 °C would fall outside of the heat transfer coefficient/heat transfer area bands. This information can be used along with Figure 5-5 to further limit the regulated helium gap thermal conductivity used in the thermal resistance network.

3. Thermal Network Coupling With TITAM

The TITAM computer code provides a means of simulating the operation of a TOPAZ-II TFE in the reactor core under both steady-state and transient conditions (Paramonov and El-Genk, 1994). Although the test stand is constructed differently than the actual core and the thermal and electrical coupling of the TFE with the actual reactor systems does not exist, the location of the collector sleeve thermocouples in the test stand does provide a means of entering TITAM and having TITAM determine the operating characteristics of the TFE.

The required inputs into the electrically heated TFE component operation portion of TITAM are thermal input power, inlet NaK coolant temperature, and NaK coolant flow rate. The thermal input power to the TFE is equal to the active zone power, P_{az}, used in the thermal network. The average collector sleeve temperature, T_6, may be used as the NaK coolant inlet temperature, and a typical NaK flow rate of 1.3 kg/s is used as the last required input to TITAM. From the inputted data, TITAM outputs the radial temperature distribution through a TFE in the reactor core and provides the output operating characteristics. The TITAM program was executed using the inputs from Table 5-1. The steady-state output and the relevant data from the thermal analysis are presented in Table 5-2.

Parameter	TITAM Output	Thermal Analysis Results
Thermal Power to TFE (W)	3,003	3,003
TFE Load Voltage (V)	0.81	1.38
Load Current (A)	184.38	78.89
Load Electric Power (W)	149.58	108.87
TFE Efficeincy (%)	4.98	3.63
Cesium Reservior Temperature (K)	576	528
Emitter Surface Temperature (K)	1,835.57	-
Collector Surface Temperature (K)	765.71	763.93
Insulator Temperature (K)	763.75	761.88
Coolant Average Temperature (K)	727.58	726.83

Table 5-2. Comparison of TITAM output to Thermal Analysis Results.

The discrepancy in the TFE output power could be the result of the differences between operating a TFE in the test stand and simulating the operation of a TFE in the reactor core. Another possible source of error are the initial and operating conditions that TITAM uses in its calculations being different from the actual test stand conditions. TITAM has a user friendly interface through two input files which can be changed to reflect various initial and operating conditions in the reactor core. This includes the ability to vary the steady-state interelectrode gap cesium pressure.

TITAM initially uses a steady-state cesium pressure of approximately 2.0 torr (based on a cesium reservoir temperature of 576 K). The input files were not altered prior to running the example data set through TITAM to obtain the above results. When TITAMs initial steady-state cesium pressure was changed to reflect the actual operating pressure in the test stand of 0.5 torr (based on a cesium reservoir temperature of 528 K), the TFE output power increased from 151 W to 188 W. Although TITAM is being used for a purpose that it was not designed for, this trend is contrary to the experimental data collected.

The TITAM temperature distribution correlates well with the thermal analysis mainly due to these calculations being based on simple heat transfer principles. This indicates that TITAM could be used to estimate the emitter surface temperature based on test stand thermal analysis data.

In order to understand the discrepancies encountered by trying to couple the experimental test stand data with TITAM, a detailed examination of how TITAM actually performs it calculations and the assumptions under which it operates is required.

VI. CONCLUSIONS

The TOPAZ-II TFE test stand provides an effective means to investigate the performance of an individual TFE without the interfering effects and complexity of the integrated TOPAZ-II system. A detailed thermal analysis is completed to better predict the behavior of a single-cell TFE and to understand the thermal losses associated with the test stand components.

Prior to developing the thermal model, extensive research of the test stand construction and materials was necessary. Due to the large volume of Russian documentation and the difficulty in translating highly technical data and engineering drawings, the development of test stand cross-sectional drawings and the determination of component materials and material properties were crucial to the thermal analysis.

A thermal resistance network has been utilized to determine the thermal loss mechanisms through each of the test stand components. Conductive heat transfer through the metal components accounts for a very small portion of the overall temperature drop from the emitter to the water channel. For the data set used in the example calculations, only 7% of the estimated temperature drop from the inner surface of the collector sleeve to the bulk water temperature occurred in the metal components.

Both radiation and conduction heat transfer occur through the regulated and unregulated helium gaps, but calculations indicate that radiation heat transfer does not contribute significantly to the total heat transferred through these gaps. The pressure in the regulated helium gap is varied during power changes to maintain the collector sleeve temperature relatively constant. Due to the very low pressure maintained in this gap (≤ 10 torr), the helium is rarefied and the thermal conductivity of the gas is not only dependent

on gas temperature but is also a function of gas pressure. Estimations based on the assumption that the cooling water is not boiling in the channel give a range of regulated helium thermal conductivities between 0.073-0.087 W/mK at a gap pressure of 10 torr. This range is approximately 30% of the thermal conductivity value calculated assuming a temperature dependence only. The regulated helium gap is one of the most critical resistances in the thermal network.

The primary mode of heat transfer into the water channel is forced convection heat transfer. Determining the amount of heat transferred into the water by forced convection requires calculating the convective heat transfer coefficient. This coefficient is dependent on the flow characteristics in the channel, the cooling channel geometry and the thermophysical properties of the cooling water. The Reynolds number is calculated to be 1480 which indicates that the flow rate is in the combined laminar flow regime. This is a very difficult regime in which to accurately calculate the heat transfer coefficient due to the importance of the buoyant, conductive and convective forces in the channel. Based on existing correlations, the convective heat transfer coefficient is determined to fall between the range of 528-1012 W/m^{2}K.

Another critical resistance in the thermal network is the cesium interelectrode gap. Conduction heat transfer occurs through the cesium vapor and can be defined in terms of the cesium vapor pressure, the gap size and the surface temperatures of the emitter and collector. Due to the high emitter temperatures, radiation heat transfer is significant through this gap. The gap heat transfer characteristics are directly affected by the thermionic process. Coupling the thermal model with a thermionic model is crucial to estimating emitter temperatures based on data collected from the test stand.

The TITAM computer code provides a means of simulating steady-state and transient operation of a TOPAZ-II TFE in the reactor core. TITAM can be utilized to

estimate the operating characteristics of a TFE in the test stand by inputting the active zone power, average collector sleeve temperature (corresponding to the NaK temperature), and an assumed NaK flow rate (based on typical values). The collector sleeve temperature calculated by TITAM is 766 K compared to a temperature of 764 K calculated using the thermal network. These temperatures calculations are based on simple heat transfer principles which provides good correlation between the two calculations. TITAM can also be used to estimate the emitter surface temperature based on the input data; however, the thermal resistance of the cesium interelectrode gap must be defined before the thermal analysis presented in this thesis can be used to provide an estimate of the emitter surface temperature to compare it to.

Differences in the TITAM output and the thermal analysis results can be attributed to several reasons. The most important of these is that TITAM simulates a TFE operating in the TOPAZ-II reactor core and not in the test stand. Several other differences include cesium reservoir temperature, TFE load voltage, TFE load current, and TFE efficiency. To understand the discrepancies between the two results requires a detailed examination of the TITAM code and integration of the thermal model developed in this thesis with the thermionic model of the code.

VII. RECOMMENDATIONS

The TOPAZ-II TFE test stand provides an excellent vehicle for investigating the thermionic characteristics of a single TFE; however, understanding the thermal characteristics of the test stand and how its thermal behavior affects the thermionic process is crucial in being able to correlate test stand results to the entire reactor core. Several improvements to the test stand and additional testing could greatly aid in improving the thermal model developed in this thesis.

A detail investigation of the flow characteristics of the cooling water would provide a better estimation of the convective heat transfer coefficient. This could include moving the inlet and outlet cooling water thermocouples inside the vacuum chamber closer to the test sections water jacket. Using more accurate temperature measurements would allow increasing the water flow rate into a better understood and documented flow regime. Testing of the cooling water characteristics could be accomplished using a known power input into the degassing heaters and would not require the operation of the TFE. Thermocouple instrumentation inside the water channel itself, would also prove useful.

Further understanding the pressure dependence of the regulated helium gap's thermal conductivity is critical to the accuracy of the thermal model. Once the thermal characteristics of the regulated helium gap and the cooling water channel are well defined, a more accurate heat balance can be performed between the collector sleeve and the cooling water.

Exploring the end effects at the upper and lower helium chambers would provide a better understanding of the 2-dimensionality of the thermal system. Experiments could easily be performed without the operation of the TFE to examine how these end chambers are affecting the axial temperature distribution along the collector sleeve. Operating the

heaters for one or both of these chambers during operation of the TFE provides an additional heat input into the thermal model; therefore, the input power to these heaters should be recorded.

Experimental information is only valuable if the accuracies of the instrumentation and data acquisition system are completely defined. The integration of Russian and American equipment is inherent to the TOPAZ project and increases the difficulty in developing an accurate model for the test stand. Improved documentation of the test stand measurement errors should accompany any future experimental work.

Experimental data should be collected from the test stand at a predetermined TFE output voltage. This voltage level should be based on supplying a specified bus voltage (i.e. 28 VDC or 30 VDC). This must be a consideration since operating the TFE at the maximum output power (or maximum efficiency) might not produce useful voltage to supply a power distribution bus.

TITAM is a valuable tool that should be modified further for use with the test stand. Utilizing the thermionic emission model from TITAM along with the thermal model developed in this thesis can provide a detailed understanding of the thermal characteristics of the test stand. This would allow for a more direct correlation of the test stand results with the operation of the overall TOPAZ-II reactor system.

APPENDIX A. THERMAL PROPERTIES

The thermal conductivities and emissivities of various test stand components are graphed and are defined in terms of temperature. Most of the information was available in Paramonov and El-Genk, 1994, but some was derived from reference book data tables. References are provided in the titles of each figure. A polynomial curve fit of the tabulated data accomplished using *Mathcad Plus 5.0* (MathSoft, Inc., 1994).
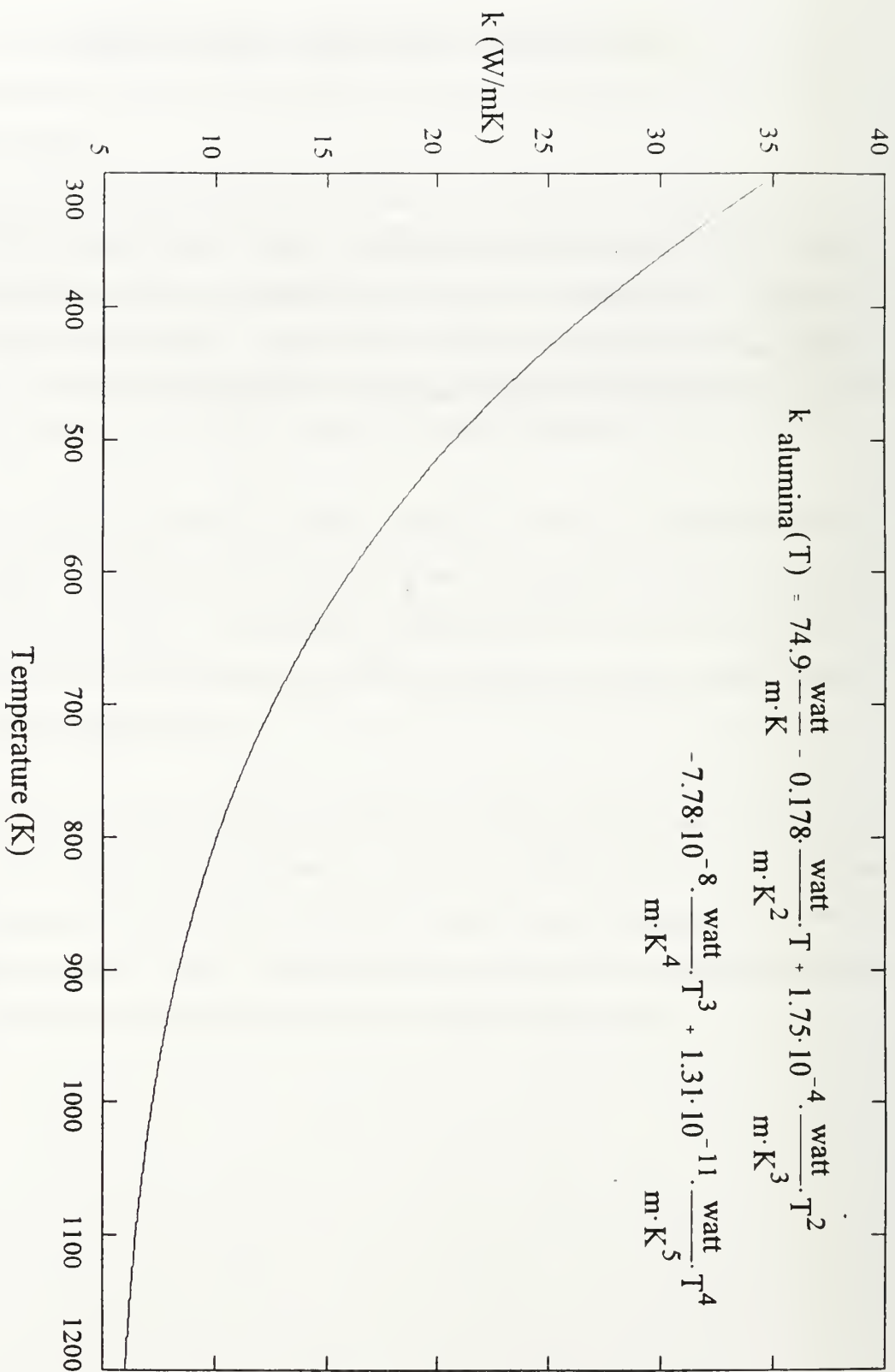
Figure A-1. Thermal Conductivity of Alumina (Al_2O_3).
(Paranomov and El-Genk, 1994)

$$k_{alumina}(T) = 74.9 \cdot \frac{watt}{m \cdot K} - 0.178 \cdot \frac{watt}{m \cdot K^2} \cdot T + 1.75 \cdot 10^{-4} \cdot \frac{watt}{m \cdot K^3} \cdot T^2$$

$$- 7.78 \cdot 10^{-8} \cdot \frac{watt}{m \cdot K^4} \cdot T^3 + 1.31 \cdot 10^{-11} \cdot \frac{watt}{m \cdot K^5} \cdot T^4$$

$$k_{Cu}(T) = 422.286 \frac{\text{watt}}{\text{m·K}} - 6.71429 \, 10^{-2} \cdot \frac{\text{watt}}{\text{m·K}^2} \cdot T$$
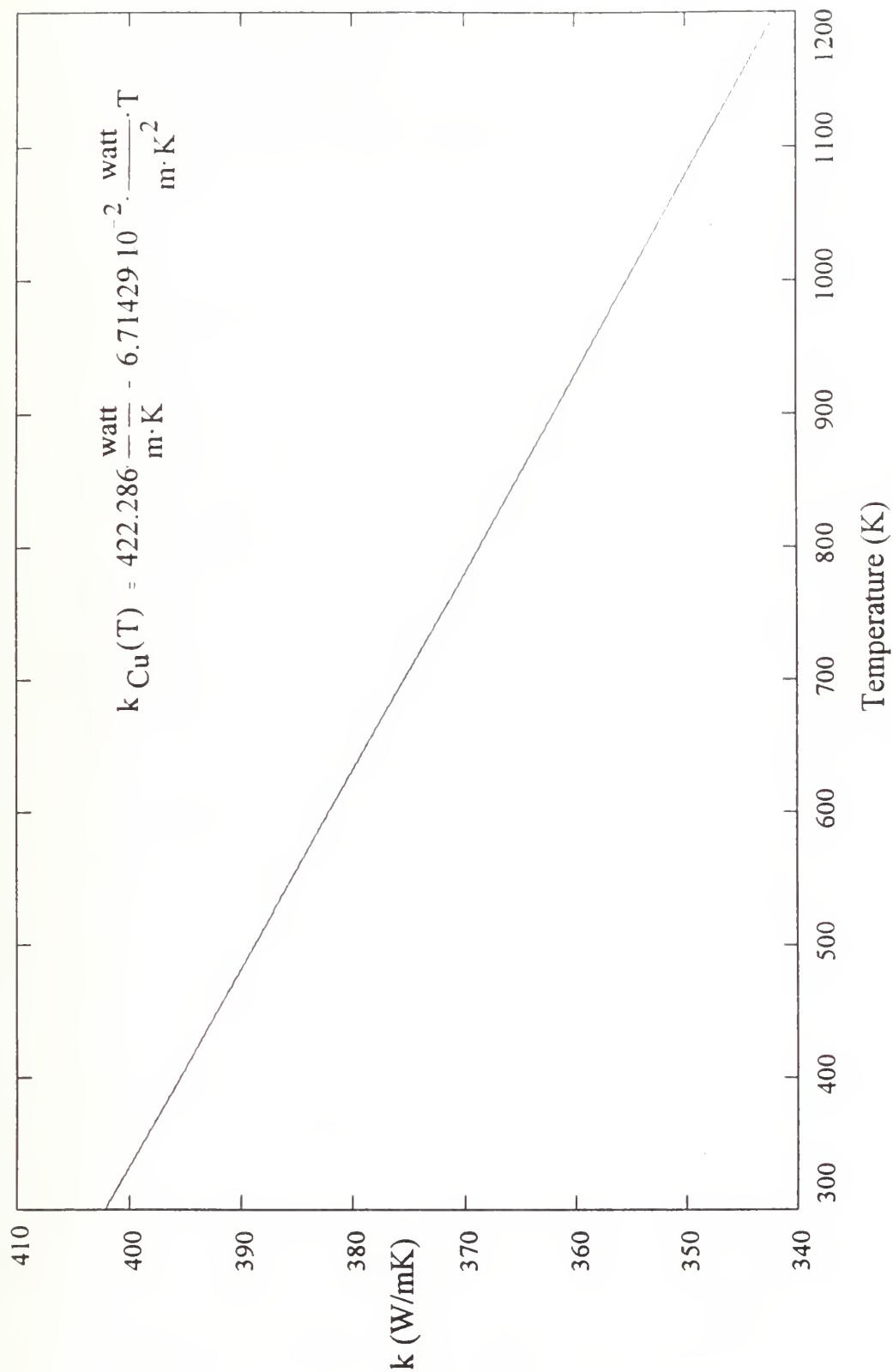
Figure A-2. Thermal Conductivity of 99.99% pure Copper.
(Powell et al., 1966)
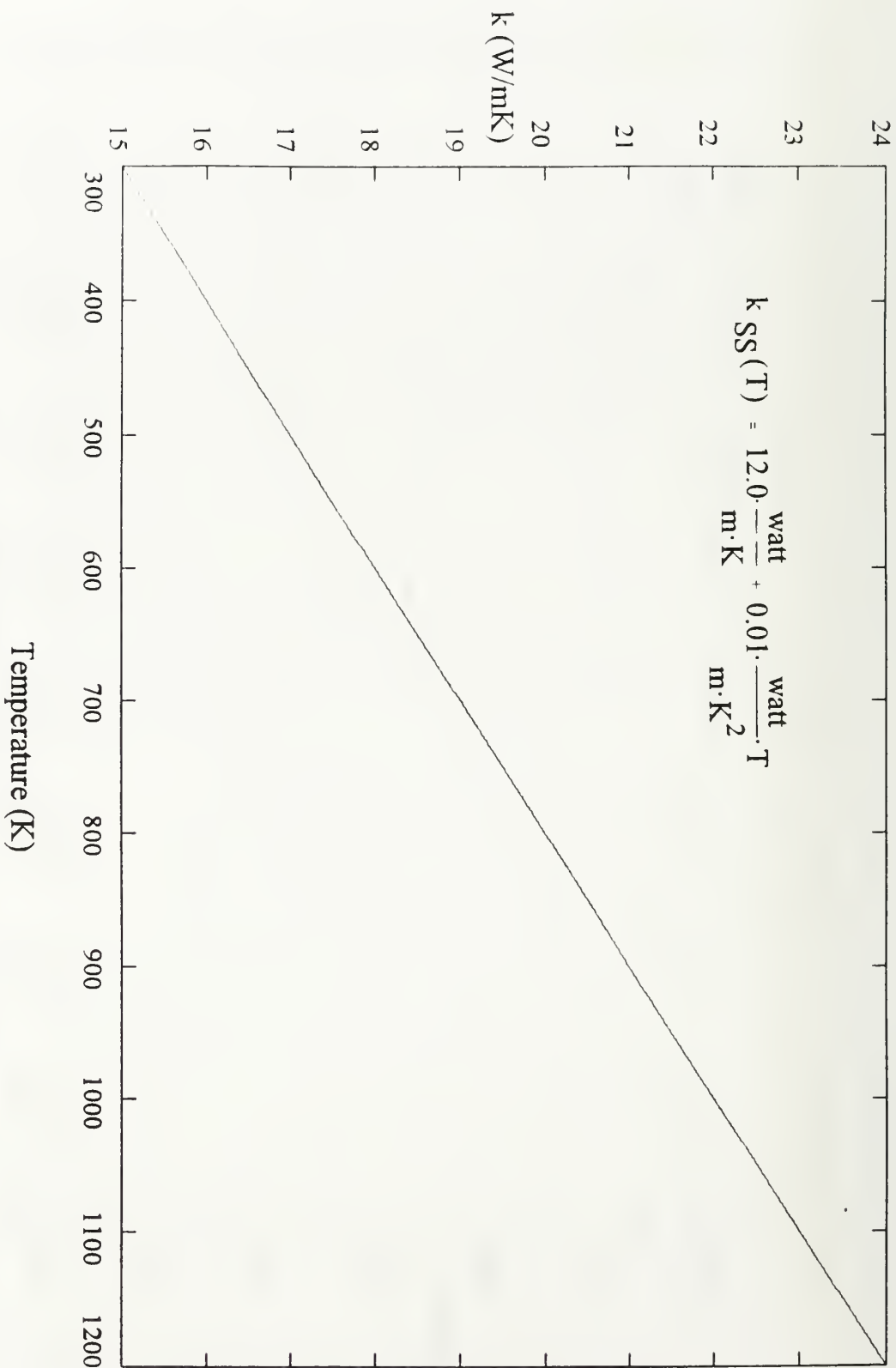
Figure A-3. Thermal Conductivity of AISI-321 Stainless Steel.
(Peckner and Bernstein, 1977)

$$k_{SS}(T) = 12.0 \cdot \frac{watt}{m \cdot K} + 0.01 \cdot \frac{watt}{m \cdot K^2} \cdot T$$

$$k_{He}(T) = -9.06 \cdot 10^{-2} \cdot \frac{watt}{m \cdot K} + 9.376 \cdot 10^{-4} \cdot \frac{watt}{m \cdot K^2} \cdot T - 9.13 \cdot 10^{-7} \cdot \frac{watt}{m \cdot K^3} \cdot T^2 \ldots$$
$$+ 5.5 \cdot 10^{-10} \cdot \frac{watt}{m \cdot K^4} \cdot T^3 - 1.264 \cdot 10^{-13} \cdot \frac{watt}{m \cdot K^5} \cdot T^4$$
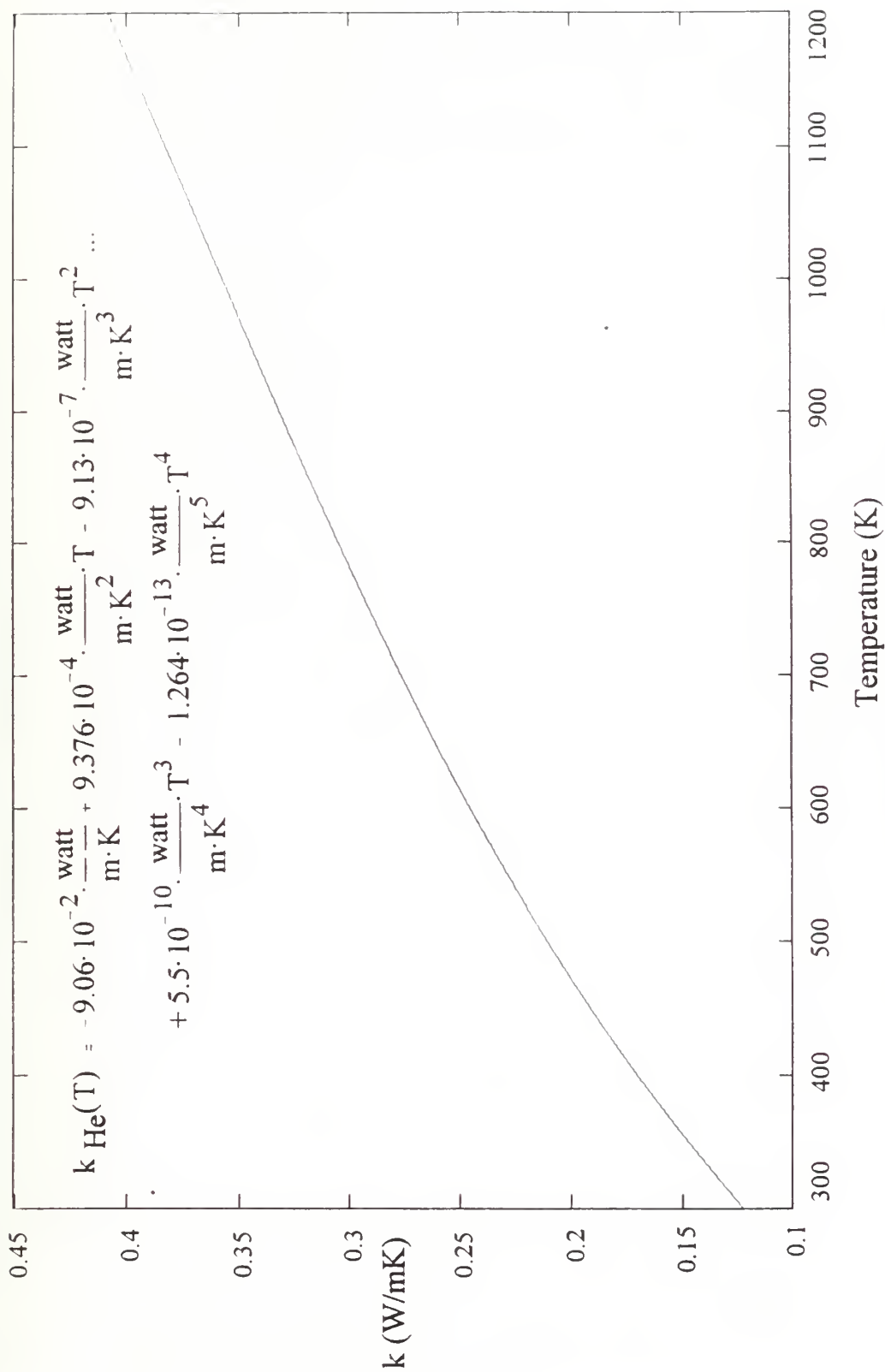
Figure A-4. Thermal Conductivity of a Helium Continum.
(Andrews and Biblarz, 1981)
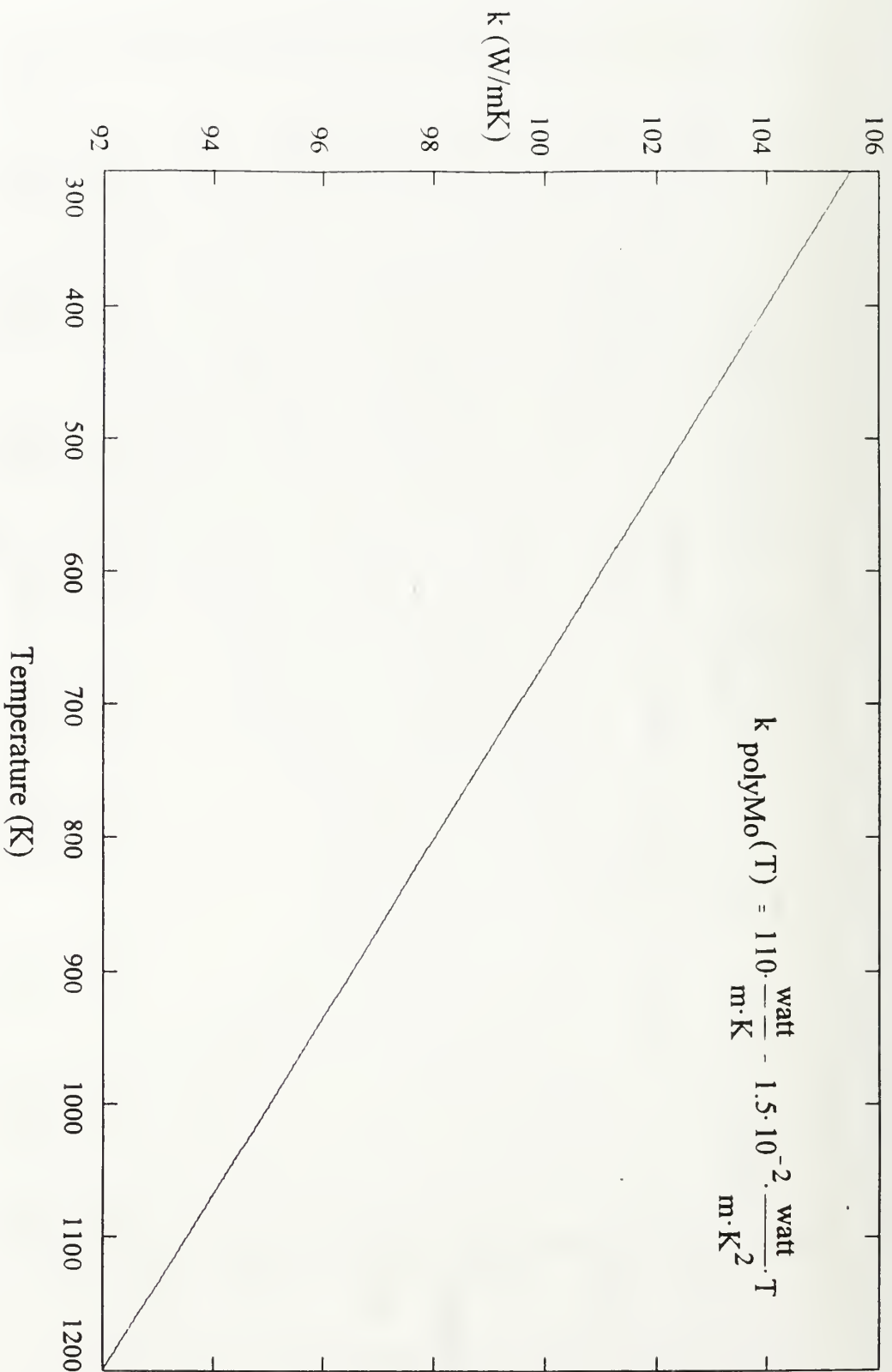
Figure A-5. Thermal Conductivity of Polycrystalline Molybdenum. (Paranomov and El-Genk, 1994)

$$k \text{ polyMo}(T) = 110 \cdot \frac{\text{watt}}{\text{m} \cdot \text{K}} - 1.5 \cdot 10^{-2} \cdot \frac{\text{watt}}{\text{m} \cdot \text{K}^2} \cdot T$$

$$\varepsilon_{ss}(T) = 0.332 - 0.00171 \cdot K^{-1} \cdot T + 5.68 \cdot 10^{-6} \cdot K^{-2} \cdot T^2$$
$$- 7.67 \cdot 10^{-9} \cdot K^{-3} \cdot T^3 + 3.69 \cdot 10^{-12} \cdot K^{-4} \cdot T^4$$
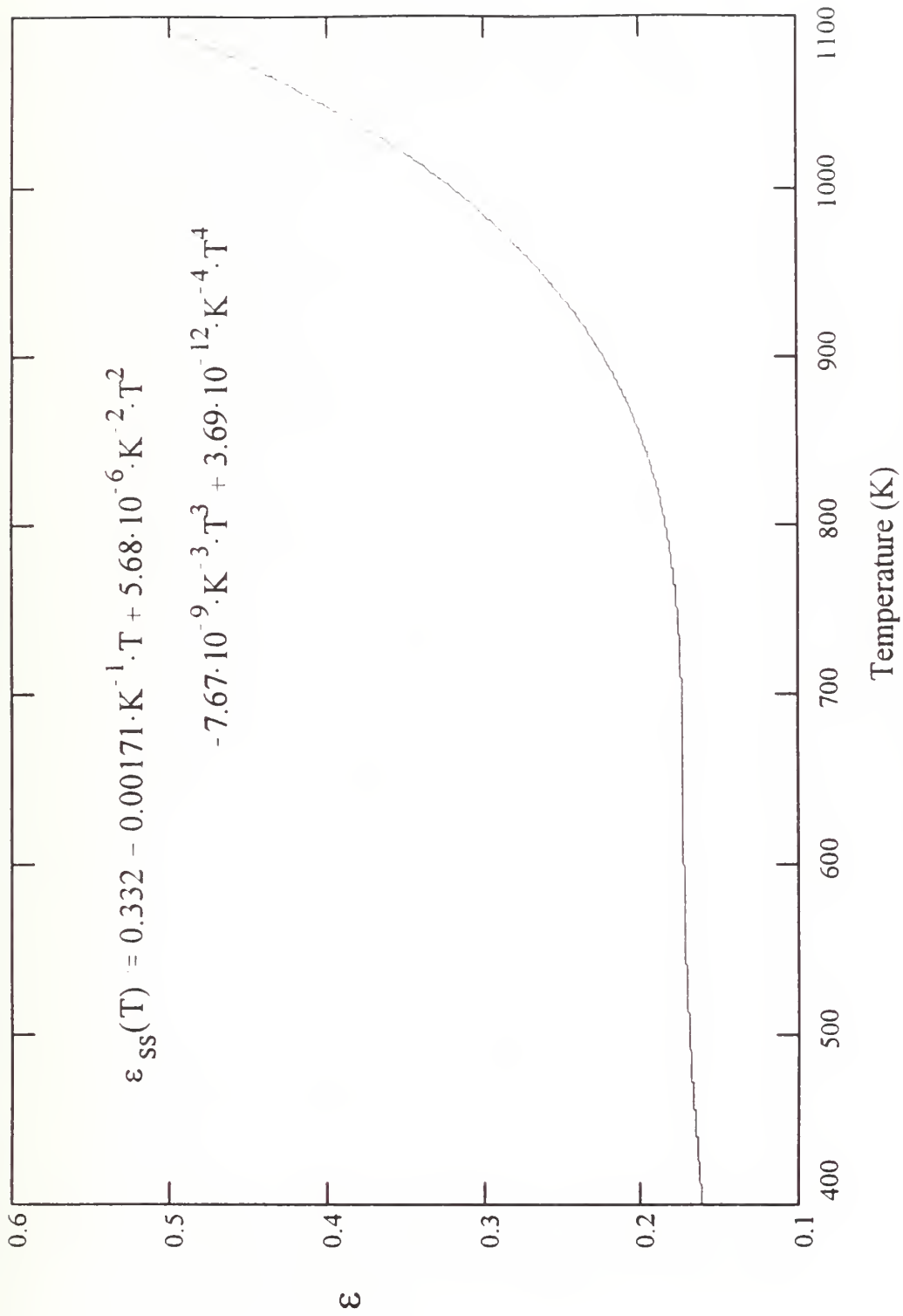
Figure A-6. Emissity of AISI-321 Stainless Steel.
(Peckner and Bernstein, 1977)
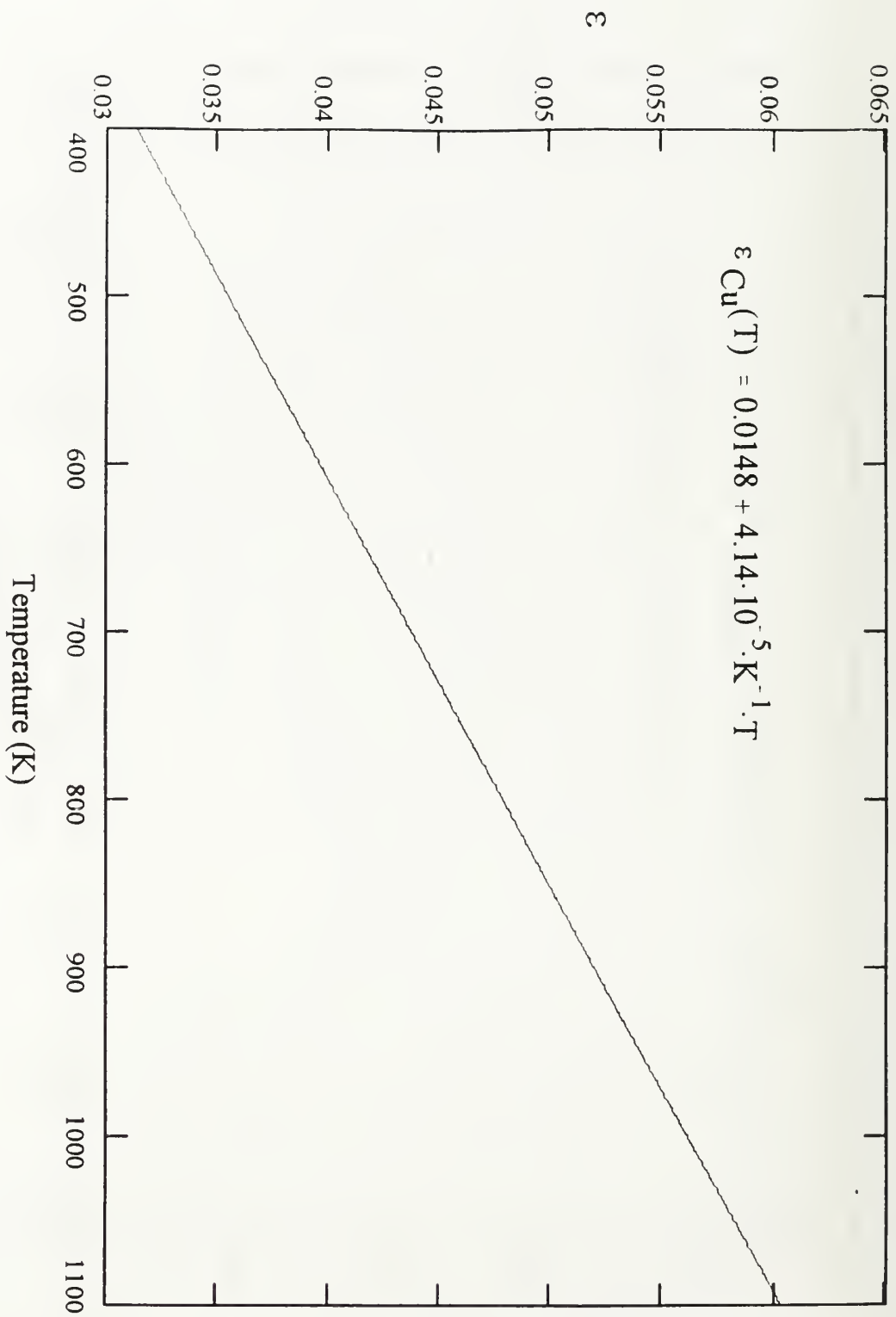
Figure A-7. Emissity of 99.99% pure Copper.
(Baumeister, 1978)

$$\varepsilon_{Cu}(T) = 0.0148 + 4.14 \cdot 10^{-5} \cdot K^{-1} \cdot T$$
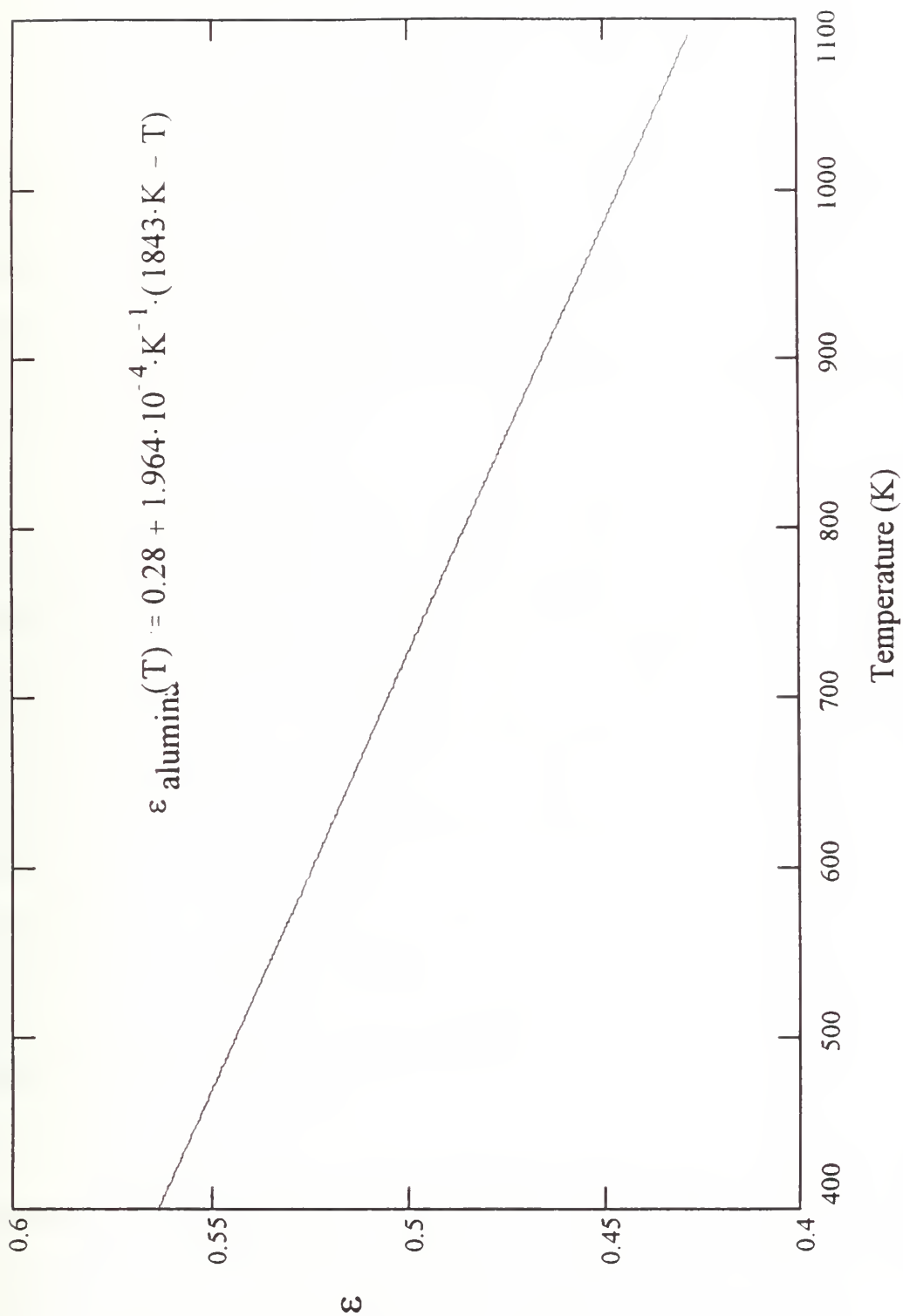
Figure A-8. Emissity of Alumina (Al_2O_3).
(Baumeister, 1978)

$$\varepsilon_{alumina}(T) = 0.28 + 1.964 \cdot 10^{-4} \cdot K^{-1} \cdot (1843 \cdot K - T)$$

APPENDIX B. EXPERIMENTAL DATA TABLES

Data were collected in support of this thesis during two separate experimental sessions. The first occurred between 15-26 March, 1994, when data were collected over a TISA heater input power range of 1000 W to 3600 W. The primary purpose of the runs completed during this period was to establish the operating characteristics of the test stand and its associated TFE from normal operating range to very low input power levels. This information is being used in a follow-on thesis to examine the thermionic characteristic of a TFE in the test stand.

The second experimental session occurred between 14-18 August, 1994. Prior to this session, the entire test stand data acquisition system was converted from a computer hardware and software system that was furnished by the Russians to a more contemporary system that was designed and assembled by the US, TIP personnel. This system update provides for much easier data acquisition and test stand control. Although the data acquisition system changed between the two experimental procedures, the test stand operating conditions were maintained as close as possible to allow for data correlation between the two collection periods. The primary purpose of the second experimental procedure was to support thermal model calculations by investigating the relationship between regulated helium gap pressure and collector sleeve temperature and to collect data a various power levels for an optimized cooling water flow rate. Relevant data to the thermal analysis are tabulated in this appendix.

The appendix is separated into three time periods, each time period consisting of three tables. The shaded columns contain data that were recorded from the test stand and the unshaded columns contain derived data. All of the data are collected at a cesium reservoir temperature of approximately 255 °C (around 0.5 torr of pressure).

71

The second column of the first table is TISA active zone power and is determined by multiplying the TISA input power by 88%. The fifth column is TFE output power and is determined by multiplying the TFE output voltage by its output current. The column indicated as column "A" is the power loss from the TFE. These values are found by subtracting the TFE output power from the TISA active zone power. TFE efficiency in column seven is the result of dividing the TFE output power by the TISA active zone power and multiplying by 100.

Column eight of the first table is the average collector sleeve temperature and is the same value as in column five of the third table. Performing a heat balance on the cooling water provides the data in the columns indicated as column "B" and "C". There is one column for each of the two output thermocouples. These values are the same values as given in columns 12 and 13 of the third table. The % error in columns 11 and 13 of the first table are the percent difference between the cooling water heat balance (columns "B" and "C") and the power balance (column "A")

The second table presents the 11 collector sleeve thermocouple measurements. See Figure 5-1 for the relative axial location of the thermocouples along the collector sleeve. Columns 2 through 6 of the third table provide relevant information concerning the thermocouple measurements. Column five gives the average of all 11 collector sleeve thermocouples and column six gives the average of thermocouples T57 through T66. This excludes the end point temperature measurements of T56 and T67.

Column eight of the third table contains the measured water flow rate (in gpm) converted to a cooling water mass flow rate (in kg/s). Columns 12 and 13 of the third table indicate the results of the cooling water heat balance (utilizing Equation 5.10).

The tables dated 13-14 August 1994 are taken over a TISA input power of 1000-3600 W. At each power level the regulated helium gap pressure was adjusted to its optimum value. This maintains a relatively constant collector sleeve temperature over the entire power range. The high % error for the 1000 W data run is due to the small temperature difference between the cooling water inlet and outlet. This indicates how sensitive the cooling water heat balance is to this temperature difference.

The tables dated 14-16 August 1994 provides data collected over three power ranges with varying regulated helium gap pressure at each power level. The first table shows that for a constant input power level, the collector sleeve temperature decreases as the regulated helium gap pressure increases. This proves how important understanding the pressure dependence of the regulated helium gap thermal conductivity is to the thermal analysis of the test stand.

The tables dated 17-18 August 1994 provides a set of data runs under similar conditions as presented in the first set of tables. A complete set of all data acquired during both experimental periods is archived at the TIP facility in Albuquerque, New Mexico.

Experimental Test Stand Data taken 13-14 August 1994

TISA Input Power W	TISA Active Zone Power W	TFE Output Voltage V	TFE Output Current A	TFE Output Power W	A Power Loss W	TFE Efficiency %	Coll. Sleeve Temp. C	Press. Reg. Helium Gap torr	B Heat Xfer'd to Water #1 W	% Error B/C %	C Heat Xfer'd to Water #2 W	% Error C/A %
1000	880	0.18	52	9.36	870.64	1.063636	472.7867	1	273.1861	68.62238	424.3491	51.26009
1200	1056	0.15	111.33	16.6995	1039.301	1.581392	526.2511	1	1027.285	1.156074	940.4465	9.511585
1200	1056	0.31	49.8	15.438	1040.562	1.461932	432.4922	1.5	877.8381	15.63808	845.0558	18.78852
1400	1232	0.23	114.99	26.4477	1205.552	2.146729	446.1656	2	1145.56	4.976292	1161.952	3.616652
1600	1408	0.39	116.46	45.4194	1362.581	3.22581	477.7056	2	1376.858	1.047827	1393.249	2.250777
1800	1584	0.48	106.93	51.3264	1532.674	3.240303	438.0644	3	1465.228	4.400529	1404.414	8.368341
2000	1760	0.57	117.92	67.2144	1692.786	3.819	445.9422	3.8	1316.757	22.21359	1322.221	21.89083
2200	1936	0.68	116.46	79.1928	1856.807	4.090537	465.9567	3.8	1509.518	18.70355	1465.175	21.0917
2400	2112	0.81	116.45	94.3326	2017.667	4.466506	457.7667	4.6	1825.464	9.526019	1842.093	8.701863
2600	2288	0.87	111.33	96.8571	2191.143	4.233265	471.8956	4.6	1551.697	29.1832	1793.922	18.12847
2800	2464	0.99	116.46	115.2954	2348.705	4.679196	447.0378	6.6	2136.843	9.020342	2192.721	6.641252
3000	2640	1.11	116.46	129.2706	2510.729	4.896614	461.2667	6.6	2387.515	4.907523	2211.356	11.92377
3200	2816	1.12	120.85	135.352	2680.648	4.806534	456.9678	8	2425.946	9.501523	2420.403	9.708298
3400	2992	1.25	115.72	144.65	2847.35	4.834559	452.5	10	2578.877	9.428871	2595.981	8.828178
3600	3168	1.27	114.26	145.1102	3022.89	4.580499	463.68	10	2786.182	7.830521	2824.718	6.555701

TISA Input Power W	T(56) C	T(57) C	T(58) C	T(59) C	T(60) C	T(61) C	T(62) C	T(63) C	T(65) C	T(66) C	T(67) C
1000	440.59	517.54	521.44	503.11	494.32	517.02	482.37	452.7	387.88	378.7	349.75
1200	507.17	589.43	569.22	557.58	544.08	5612	528.3	510.01	444.79	431.65	407
1200	405.36	480.99	483.55	463.93	450.04	471.68	434.45	415.56	350.38	341.85	316.64
1400	427.6	505.56	484.56	478.98	467.34	472.29	443.52	429.17	371.3	362.77	340.76
1600	464.25	551.5	512.31	517.02	494.52	508.14	467.63	461.34	400.21	386.68	368.27
1800	416.28	511.45	472.07	472.64	449.16	469.39	424.86	423.3	366.07	353.64	335.13
2000	423.64	518.51	478.85	478.54	465.36	475.22	427	422.51	379.72	367.77	352.26
2200	449.39	539.44	495.87	511.27	483.95	497.94	437.74	443.61	399.35	384.44	367
2400	447.91	543.85	486.15	502.28	475.23	489.37	431.05	437.27	384.25	370.45	352.51
2600	476.21	553.49	496.16	513.34	489.54	503.37	437.93	454.98	405.51	392.74	373.2
2800	429.52	528.44	474.66	490.49	472.18	481.28	415.75	425.58	373.06	361.9	342.04
3000	445.41	549.5	494.18	509.7	478.32	498.46	412.51	442.55	390.01	376.17	357.41
3200	448.15	541.07	486.84	499.12	483.93	488.77	418.6	436.39	385.44	372.55	355.33
3400	433.38	527.7	487.88	487.36	488.08	486.75	415.59	434.22	378.59	366.33	352.05
3600	450.35	543.47	497.14	502.08	488.39	503.43	416.31	450.23	393.22	378.85	363.85

TISA Input Power W	Minimum Temperature C	Maximum Temperature C	Max/Min Ave. Temp. C	Coll. Sleeve Ave. Temp. w/ T(56/67)	Coll. Sleeve Ave. Temp. w/o T(56/67)	Water Flowrate gpm	Water Mass Flowrate kg/s	Water In. Temp. C	Water Out Temp. #1 C	Water Out Temp. #2 C	Heat Xferr'd to Water #1 W	Heat Xferr'd to Water #2 W
1000	349.75	521.44	435.595	458.6745	472.7867	0.69	0.043518	13.12	14.62	15.45	273.1861	424.3491
1200	407	589.43	498.215	513.6755	526.2511	0.7	0.044149	11.78	17.34	16.87	1027.285	940.4465
1200	316.64	483.55	400.095	419.4936	432.4922	0.69	0.043518	11.94	16.76	16.58	877.8381	845.0558
1400	340.76	505.56	423.16	434.8955	446.1656	0.69	0.043518	11.18	17.47	17.56	1145.56	1161.952
1600	368.27	551.5	459.885	466.5336	477.7056	0.69	0.043518	11.04	18.6	18.69	1376.858	1393.249
1800	335.13	511.45	423.29	426.7264	438.0644	0.72	0.04541	10.59	18.3	17.98	1465.228	1404.414
2000	352.26	518.51	435.385	435.3982	445.9422	0.69	0.043518	24.37	31.6	31.63	1316.757	1322.221
2200	367	539.44	453.22	455.4545	465.9567	0.7	0.044149	24.95	33.12	32.88	1509.518	1465.175
2400	352.51	543.85	448.18	447.3018	457.7667	0.7	0.044149	10.52	20.4	20.49	1825.464	1842.093
2600	373.2	553.49	463.345	463.3155	471.8956	0.69	0.043518	25.21	33.73	35.06	1551.697	1793.922
2800	342.04	528.44	435.24	435.9	447.0378	0.73	0.046041	10.81	21.9	22.19	2136.843	2192.721
3000	357.41	549.5	453.455	450.3836	461.2667	0.71	0.04478	9.77	22.51	21.57	2387.515	2211.356
3200	355.33	541.07	448.2	446.9264	456.9678	0.7	0.044149	9.59	22.72	22.69	2425.946	2420.403
3400	352.05	527.7	439.875	441.63	452.5	0.72	0.04541	10.39	23.96	24.05	2578.877	2595.981
3600	363.85	543.47	453.66	453.3927	463.68	0.73	0.046041	10.21	24.67	24.87	2786.182	2824.718

Experimental Test Stand Data taken 14-16 August 1994

TISA Input Power W	TISA Active Zone Power W	TFE Output Voltage V	TFE Output Current A	TFE Output Power W	A Power Loss W	TFE Efficiency %	Coll. Sleeve Temp. C	Press. Reg. Helium Gap torr	B Heat Xferr'd to Water #1 W	% Error B/C %	C Heat Xferr'd to Water #2 W	% Error C/A %
1400	1232	0.44	54.2	23.848	1208.152	1.935714	535.199	1	1064.238	11.9119	1091.953	9.61794
1400	1232	0.25	79.83	19.9575	1212.043	1.619927	315.288	5	1067.881	11.89413	1134.079	6.432426
2400	2112	0.76	144.29	109.6604	2002.34	5.192254	578.163	2	1960.236	2.102728	2037.071	1.734546
2400	2112	0.94	114.26	107.4044	2004.596	5.085436	381.158	10	1843.94	8.014346	1927.084	3.866696
2400	2112	0.67	143.55	96.1785	2015.822	4.553906	333.294	16	1875.72	6.950109	1830.11	9.21272
2400	2112	0.67	147.22	98.6374	2013.363	4.670331	323.742	18	1801.603	10.5177	1985.944	1.361813
2400	2112	0.66	145.02	95.7132	2016.287	4.531875	317.745	19	1942.235	3.672702	1908.027	5.369269
2400	2112	0.63	146.48	92.2824	2019.718	4.369432	316.662	20	1849.668	8.419472	1821.558	9.811273
3400	2992	1.31	90.76	118.8956	2873.104	3.973783	610.2611	3	1489.775	48.14755	2007.007	30.14499
3400	2992	1.33	112.06	149.0398	2842.96	4.981277	519.4933	5	2285.578	19.6057	2285.578	19.6057
3400	2992	1.67	52	86.84	2905.16	2.902406	445.4422	10	2305.849	20.62918	2367.613	18.50318
3400	2992	1.69	45.41	76.7429	2915.257	2.564936	385.9211	10	2264.673	22.31651	2233.316	23.39213
3400	2992	1.05	112.79	118.4295	2873.571	3.958205	384.9478	20	2527.882	12.02992	2569.771	10.5722
3400	2992	0.88	112.79	99.2552	2892.745	3.317353	325.2111	39	2454.558	15.1478	2531.208	12.49805

76

TISA Input Power W	T(56) C	T(57) C	T(58) C	T(59) C	T(60) C	T(61) C	T(62) C	T(63) C	T(65) C	T(66) C	T(67) C
1400	528.65	614.94	598.48	592.21	563.23	594.99	544.65	537.08	454.44	437.5	414.47
1400	282.12	332.26	373.8	321.35	352.79	374.82	340.53	309.53	256.73	255.75	235.32
2400	591	689.7	616.54	652.35	615.25	633.65	557.4	589.02	495.56	472.16	460
2400	357.2	415.22	450.84	402.8	437.2	442.49	409.68	386.24	295.84	288.66	282.61
2400	315.36	359.79	382.98	345.7	374.67	376.01	364.71	345.88	264.65	259.26	259.29
2400	313.86	349.87	372.24	329.82	355.99	374.67	336.46	349.31	260.09	254.32	254.65
2400	304.09	338.61	359.98	330	354.21	356.03	347.09	329.94	256.84	252.08	252.67
2400	303.81	331.16	355.89	328.25	354.22	360.52	342.11	337.77	255.67	249.35	251.68
3400	608.78	712.25	630.72	664.16	636.26	646.43	554.14	591.4	539.6	517.39	500.44
3400	521.47	627.3	543.27	577.1	544.65	548.84	468.76	496.05	440.55	428.92	397
3400	433.42	521.84	485	495.73	474.37	488.42	406.22	425.92	360.66	350.82	333.95
3400	354.85	411.72	430.16	397.42	421.2	430.13	403.79	380.3	303.26	295.31	293.39
3400	359.54	410.27	430.11	390.61	421.73	428.75	403.3	380.29	303.96	295.51	294.32
3400	299.85	342.15	346.58	329.43	338.63	352.15	341.8	338.92	272.44	264.8	272.95

TISA Input Power W	Minimum Temperature C	Maximum Temperature C	Max/Min Ave. Temp. C	Coll. Sleeve Ave. Temp. w/ T(56/67) C	Coll. Sleeve Ave. Temp w/o T(56/67)	Water Flowrate gpm	Water Mass Flowrate kg/s	Water In. Temp. C	Water Out Temp. #1 C	Water Out. Temp. #2 C	Heat Xferr'd to Water #1 W	Heat Xferr'd to Water #2 W
1400	414.47	614.94	514.705	534.6036	535.199	0.7	0.044149	10.58	16.34	16.49	1064.238	1091.953
1400	235.32	374.82	305.07	312.2727	315.288	0.66	0.041626	36.85	42.98	43.36	1067.881	1134.079
2400	460	689.7	574.85	579.33	578.163	0.71	0.04478	26.55	37.01	37.42	1960.236	2037.071
2400	282.61	450.84	366.725	378.98	381.158	0.7	0.044149	26.85	36.83	37.28	1843.94	1927.084
2400	259.26	382.98	321.12	331.6636	333.294	0.72	0.04541	28.06	37.93	37.69	1875.72	1830.11
2400	254.32	374.67	314.495	322.8436	323.742	0.72	0.04541	27.86	37.34	38.31	1801.603	1985.944
2400	252.08	359.98	306.03	316.5036	317.745	0.72	0.04541	28.39	38.61	38.43	1942.235	1908.027
2400	249.35	360.52	304.935	315.4936	316.662	0.71	0.04478	27.78	37.65	37.5	1849.668	1821.558
3400	500.44	712.25	606.345	600.1427	610.2611	0.69	0.043518	27.78	35.96	38.8	1489.775	2007.007
3400	397	627.3	512.15	508.5373	519.4933	0.66	0.041626	7.17	20.29	20.29	2285.578	2285.578
3400	333.95	521.84	427.895	434.2136	445.4422	0.65	0.040996	7.03	20.47	20.83	2305.849	2367.613
3400	293.39	430.16	361.775	374.6845	385.9211	0.66	0.041626	7.56	20.56	20.38	2264.673	2233.316
3400	294.32	430.11	362.215	374.3991	384.9478	0.69	0.043518	8.43	22.31	22.54	2527.882	2569.771
3400	264.8	352.15	308.475	318.1545	325.2111	0.66	0.041626	7.39	21.48	21.92	2454.558	2531.208

Experimental Test Stand Data taken 17-18 August 1994

TISA Input Power W	TISA Active Zone Power W	TFE Output Voltage V	TFE Output Current A	TFE Output Power W	A Power Loss W	TFE Efficiency %	Coll. Sleeve Temp. C	Press. Reg. Helium Gap torr	B Heat Xfer'd to Water #1 W	% Error B/C %	C Heat Xfer'd to Water #2 W	% Error C/A %
1209	1063.92	0.13	83.29	10.8277	1053.092	1.017717	418.5578	1.5	722.4255	31.3996	960.7705	8.76673
1408	1239.04	0.39	54.72	21.3408	1217.699	1.722366	478.3222	1.5	1242.482	2.03523	1070.071	12.1235
1609	1415.92	0.48	75.96	36.4608	1379.459	2.575061	469.5856	2	1489.854	8.002774	1401.775	1.617704
1800	1584	0.6	75.23	45.138	1538.862	2.849621	459.8089	2.5	1611.666	4.73104	1611.666	4.73104
2000	1760	0.69	75.23	51.9087	1708.091	2.949358	ERR	3	1555.709	8.921191	1649.939	3.404541
2200	1936	0.77	78.16	60.1832	1875.817	3.108636	453.7822	3.5	1731.235	7.707693	1762.644	6.033233
2419	2128.72	1.11	74.5	82.695	2046.025	3.884729	465.2667	4	2036.094	0.483356	1980.665	3.194466
2597	2285.36	1.21	73.03	88.3663	2196.994	3.866625	457.1767	4.8	2008.38	8.585084	2198.686	0.077047
2800	2464	1.31	78.89	103.3459	2360.654	4.194233	449.4911	6.5	2394.536	1.435268	2372.364	0.496052
3002	2641.76	1.38	74.5	102.81	2538.95	3.891724	462.7022	6.5	2411.165	5.033005	2503.546	1.394423
3214	2828.32	1.44	74.5	107.28	2721.04	3.793064	458.5244	8	2620.845	3.68224	2672.13	1.79748
3412	3002.56	1.38	78.89	108.8682	2893.692	3.625846	453.6789	10	2839.314	1.879167	2828.387	2.256797
3600	3168	0.35	272.98	95.543	3072.457	3.015878	462.4178	10	3145.283	2.370284	3107.037	1.12548

TISA Input Power W	T(56) C	T(57) C	T(58) C	T(59) C	T(60) C	T(61) C	T(62) C	T(63) C	T(65) C	T(66) C	T(67) C
1209	431.45	512.8	511.1	483.82	476.07	491.47	461.05	454.47	390.14	376.24	365.05
1408	462.43	543.42	523.85	513.95	490.98	504.61	473.39	462.55	405.85	386.3	379.88
1609	452.1	533.24	513.11	503.92	491.73	492.76	467.39	456.2	394.22	373.7	370.98
1800	443.61	525.89	499.78	501.28	475.93	482.52	450.69	450.69	386.21	365.29	363.6
2000	433.96	524.2	489.06	497.4	477.69	485.31	447.14	439.13	379	359.4	357.5
2200	434.74	531.97	484.42	499.06	479.76	477.86	438.64	429.03	381.27	362.03	358.23
2419	449.1	539.37	497.4	512.65	486.7	498.46	447.6	446.22	390.54	368.46	367.15
2597	444.27	534.41	490	500.01	479.84	488.45	434.64	436.26	384.64	366.34	358.83
2800	432.07	515.38	482.46	487.64	471.55	482.72	427.03	427.72	374.29	376.63	350.45
3002	448.67	538.92	496.24	505.56	486.26	495.53	436.52	440.98	390.55	373.76	363.74
3214	437.07	532.15	500.99	490.18	492.56	490.87	436.03	435.33	382.51	366.1	357.91
3412	424.49	515.64	498.46	483.9	482.57	490.12	433.73	439.32	376.42	362.95	354.29
3600	454.29	530.71	501.85	500.3	494.11	503.89	437.47	428.22	389.78	375.43	364.07

TISA Input Power W	Minimum Temperature C	Maximum Temperature C	Max/Min Ave. Temp. C	Coll. Sleeve Ave. Temp. w/ T(56/67)	Coll. Sleeve Ave. Temp w/o T(56/67)	Water Flowrate gpm	Water Mass Flowrate kg/s	Water In. Temp. C	Water Out Temp. #1 C	Water Out Temp. #2 C	Heat Xferr'd to Water #1 W	Heat Xferr'd to Water #2 W
1209	365.05	512.8	438.925	414.8655	418.5578	0.7	0.044149	15.18	19.09	20.38	722.4255	960.7705
1408	379.88	543.42	461.65	467.9282	478.3222	0.71	0.04478	14.23	20.86	19.94	1242.482	1070 071
1609	370.98	533.24	452.11	459.0318	459.8089	0.71	0.04478	13.97	21.92	21.45	1489 854	1401 775
1800	363.6	525.89	444.745	449.59	469.5856	0.71	0.04478	14.57	23.17	23.17	1611.666	1611 666
2000	357.5	524.2	440.85	444.5264	453.7822	0.7	0.044149	14.62	23.04	23.55	1555.709	1649.939
2200	358.23	531.97	445.1	443.3645	465.2667	0.7	0.044149	15.24	24.61	24.78	1731.235	1762.644
2419	367.15	539.37	453.26	454.8773	457.1767	0.7	0.044149	15.24	26.26	25.96	2036.094	1980 665
2597	358.83	534.41	446.62	447.0627	449.4911	0.7	0.044149	14.6	25.47	26.5	2008.38	2198.686
2800	350.45	515.38	432.915	438.9036	462.7022	0.7	0.044149	15.22	28.18	28.06	2394 536	2372.364
3002	363.74	538.92	451.33	452.43	458.5244	0.7	0.044149	15.07	28.12	28.62	2411.165	2503.546
3214	357.91	532.15	445.03	447.4273	453.6789	0.67	0.042257	15.06	29.88	30.17	2620.845	2672.13
3412	354.29	515.64	434.965	441.99		0.69	0.043518	16.56	32.15	32.09	2839.314	2828.387
3600	364.07	530.71	447.39	452.7382	462.4178	0.69	0.043518	15.86	33.13	32.92	3145.283	3107 037

APPENDIX C. THERMAL NETWORK CALCULATIONS

The following calculations and the calculations in Appendix D were completed using *Mathcad Plus 5.0* (Mathsoft, Inc. 1994). This calculational software uses a colon followed by an equal sign (:=) to mean "defined by" vice an equal sign (=) to mean "equal to". All variables must be defined prior to being used in an equation. After a variable is defined, an equal sign can be used to determine the variables value.

A.   THERMAL MODEL INPUTS

1. INPUT POWER TO THE TISA HEATER

$$Q_{TISA} := 3412 \cdot watt$$

2. POWER TO THE ACTIVE ZONE

$$Q_{az} := Q_{TISA} \cdot 0.88 \qquad Q_{az} = 3.003 \cdot 10^3 \cdot watt$$

3. TFE OUTPUT POWER

$$P_{out} := 108.9 \cdot watt$$

4. POWER LOSS FROM TFE

$$Q_{loss} := Q_{az} - P_{out} \qquad Q_{loss} = 2.894 \cdot 10^3 \cdot watt$$

5. RADIAL DIMENSIONS FOR THE TEST STAND

$r_1 = 0.0098 \cdot m$ $r_4 = 0.0119 \cdot m$ $r_7 = 0.01495 \cdot m$ $r_{10} := 0.0300 \cdot m$

$r_2 = 0.0103 \cdot m$ $r_5 = 0.01195 \cdot m$ $r_8 := 0.0150 \cdot m$ $r_{11} := 0.0325 \cdot m$

$r_3 = 0.01175 \cdot m$ $r_6 = 0.01370 \cdot m$ $r_9 = 0.0295 \cdot m$ $r_{12} := 0.0375 \cdot m$

6. LENGTH OF THE TEST SECTION

$$z := 0.3 \cdot m$$

7. DIMENSIONAL CONSTANT FOR CALCULATIONS

$$c := 2 \cdot \pi \cdot z \qquad c = 1.885 \cdot m$$

81

8. COLLECTOR SLEEVE AXIAL TEMPERATURE DISTRIBUTION

$T_{56} = 424.49 \cdot K$ $T_{59} = 483.9 \cdot K$ $T_{62} = 433.73 \cdot K$ $T_{66} = 362.95 \cdot K$

$T_{57} = 515.64 \cdot K$ $T_{60} = 482.57 \cdot K$ $T_{63} = 439.32 \cdot K$ $T_{67} = 354.29 \cdot K$

$T_{58} = 498.46 \cdot K$ $T_{61} = 490.12 \cdot K$ $T_{65} = 376.42 \cdot K$

9. AVERAGE COLLECTOR SLEEVE TEMPERATURE

The average collector sleeve temperature is calculated without using the end point temperatures, $T(56)$ and $T(67)$.

$$T_{6c} = \frac{T_{57} + T_{58} + T_{59} + T_{60} + T_{61} + T_{62} + T_{63} + T_{65} + T_{66}}{9}$$

$T_6 = T_{6c} + 273.15 \cdot K$ $T_6 = 726.829 \cdot K$

B.   FROM THE COLLECTOR SLEEVE OUTWARD

1. STAINLESS STEEL COLLECTOR SLEEVE

a. Thermal Conductivity of Stainless Steel

$$k_{SS} = 12.0 \cdot \left(\frac{watt}{m \cdot K}\right) + 0.01 \cdot \left(\frac{watt}{m \cdot K^2}\right) \cdot T_6 \qquad k_{SS} = 19.268 \cdot \frac{watt}{m \cdot K}$$

b. Temperature Drop Across Collector Sleeve

$$\Delta T_{SS} = \frac{Q_{loss} \cdot \ln\left(\frac{r_7}{r_6}\right)}{c \cdot k_{SS}} \qquad \Delta T_{SS} = 6.957 \cdot K$$

c. Temperature at node 7

$T_7 = T_6 - \Delta T_{SS}$ $T_7 = 719.872 \cdot K$

2. UNREGULATED HELIUM GAP

a. Thermal Conductivity of a Helium Continuum

$$k_{He1} = 9.376 \cdot 10^{-4} \cdot \left(\frac{watt}{m \cdot K^2} \right) \cdot T_7 - 9.13 \cdot 10^{-7} \cdot \left(\frac{watt}{m \cdot K^3} \right) \cdot T_7^2$$

$$k_{He2} = 5.5 \cdot 10^{-10} \cdot \left(\frac{watt}{m \cdot K^4} \right) \cdot T_7^3 - 1.264 \cdot 10^{-13} \cdot \left(\frac{watt}{m \cdot K^5} \right) \cdot T_7^4$$

$$k_{He} = -9.06 \cdot 10^{-2} \cdot \left(\frac{watt}{m \cdot K} \right) + k_{He1} + k_{He2} \qquad k_{He} = 0.282 \cdot \frac{watt}{m \cdot K}$$

b. Temperature Drop Across the Unregulated Helium Gap

$$\Delta T_{He} = \frac{Q_{loss} \cdot \ln \left(\frac{r_8}{r_7} \right)}{c \cdot k_{He}} \qquad \Delta T_{He} = 18.147 \cdot K$$

c. Temperature at Node 8

$$T_8 = T_7 - \Delta T_{He} \qquad T_8 = 701.725 \cdot K$$

3. COPPER CONDUCTOR

a. Thermal Conductivity of Copper

$$k_{Cu} = 422.286 \cdot \frac{watt}{m \cdot K} - 6.71429 \cdot 10^{-2} \cdot \left(\frac{watt}{m \cdot K^2} \right) \cdot T_8 \qquad k_{Cu} = 375.17 \cdot \frac{watt}{m \cdot K}$$

b. Temperature Drop Across the Copper Conductor

$$\Delta T_{Cu} = \frac{Q_{loss} \cdot \ln\left(\frac{r_9}{r_8}\right)}{c \cdot k_{Cu}} \qquad \Delta T_{Cu} = 2.767 \cdot K$$

c. Temperature at Node 9

$$T_9 = T_8 - \Delta T_{Cu} \qquad T_9 = 698.958 \cdot K$$

4. REGULATED HELIUM GAP

The thermal conductivity of the helium in the regulated gap is first estimated using the equation for a continuum gas.

a. Thermal Conductivity of a Helium Continuum

$$k_{He3} = 9.376 \cdot 10^{-4} \cdot \left(\frac{watt}{m \cdot K^2}\right) \cdot T_9 - 9.13 \cdot 10^{-7} \cdot \left(\frac{watt}{m \cdot K^3}\right) \cdot T_9^2$$

$$k_{He4} = 5.5 \cdot 10^{-10} \cdot \left(\frac{watt}{m \cdot K^4}\right) \cdot T_9^3 - 1.264 \cdot 10^{-13} \cdot \left(\frac{watt}{m \cdot K^5}\right) \cdot T_9^4$$

$$k_{Hereg} = -9.06 \cdot 10^{-2} \cdot \left(\frac{watt}{m \cdot K}\right) + k_{He3} + k_{He4} \qquad k_{Hereg} = 0.276 \cdot \frac{watt}{m \cdot K}$$

b. Temperature Drop Across the Regulated Helium Gap

$$\Delta T_{Hereg} = \frac{Q_{loss} \cdot \ln\left(\frac{r_{10}}{r_9}\right)}{c \cdot k_{Hereg}} \qquad \Delta T_{Hereg} = 93.366 \cdot K$$

84

c. Temperature at Node 10 Based on a Helium Continuum in the Gap

$$T_{10cont} = T_9 - \Delta T_{Hereg} \qquad T_{10cont} = 605.592 \cdot K$$

This temperature will lead to a water channel inner wall temperature of around 325 °C. Since this is approximately 200 °C higher than the boiling point of water, the helium thermal conductivity must be much lower than its continuum value. From Figure 5-5, the helium thermal conductivity is estimated to be 0.08 W/mK for a wall temperature of 80 °C. Using a temperature range of 80 ± 30 °C gives a low thermal conductivity of 0.073 W/mK and a high thermal conductivity of 0.087 W/mK. The temperature drop across the regulated helium gap is recalculated based on the low, estimated, and high thermal conductivities.

d. Estimated Temperature Drop Across the Regulated Helium Gap

$$k_{Helow} = 0.073 \cdot \frac{watt}{m \cdot K} \qquad \Delta T_{Helow} = \frac{Q_{loss} \cdot \ln\left(\frac{r_{10}}{r_9}\right)}{c \cdot k_{Helow}} \qquad \Delta T_{Helow} = 353.441 \cdot K$$

$$k_{Heest} = 0.08 \cdot \frac{watt}{m \cdot K} \qquad \Delta T_{Heest} = \frac{Q_{loss} \cdot \ln\left(\frac{r_{10}}{r_9}\right)}{c \cdot k_{Heest}} \qquad \Delta T_{Heest} = 322.515 \cdot K$$

$$k_{Hehigh} = 0.087 \cdot \frac{watt}{m \cdot K} \qquad \Delta T_{Hehigh} = \frac{Q_{loss} \cdot \ln\left(\frac{r_{10}}{r_9}\right)}{c \cdot k_{Hehigh}} \qquad \Delta T_{Hehigh} = 296.565 \cdot K$$

e. Estimated Temperature at Node 10

$$T_{10low} = T_9 - \Delta T_{Helow} \qquad T_{10low} = 345.517 \cdot K$$

$$T_{10} = T_9 - \Delta T_{Heest} \qquad T_{10} = 376.443 \cdot K$$

$$T_{10high} = T_9 \quad \Delta T_{Hehigh} \qquad T_{10high} = 402.393 \cdot K$$

5. Stainless Steel Water Jacket

a. Thermal Conductivity of Stainless Steel

$$k_{wjlow} = 12.0 \cdot \left(\frac{watt}{m \cdot K}\right) + 0.01 \cdot \left(\frac{watt}{m \cdot K^2}\right) \cdot T_{10low} \qquad k_{wjlow} = 15.455 \cdot \frac{watt}{m \cdot K}$$

$$k_{wj} = 12.0 \cdot \left(\frac{watt}{m \cdot K}\right) + 0.01 \cdot \left(\frac{watt}{m \cdot K^2}\right) \cdot T_{10} \qquad k_{wj} = 15.764 \cdot \frac{watt}{m \cdot K}$$

$$k_{wjhigh} = 12.0 \cdot \left(\frac{watt}{m \cdot K}\right) + 0.01 \cdot \left(\frac{watt}{m \cdot K^2}\right) \cdot T_{10high} \qquad k_{wjhigh} = 16.024 \cdot \frac{watt}{m \cdot K}$$

b. Temperature Drop Across the Water Jacket

$$\Delta T_{wjlow} = \frac{Q_{loss} \cdot \ln\left(\frac{r_{11}}{r_{10}}\right)}{c \cdot k_{wjlow}} \qquad \Delta T_{wjlow} = 7.95 \cdot K$$

$$\Delta T_{wj} = \frac{Q_{loss} \cdot \ln\left(\frac{r_{11}}{r_{10}}\right)}{c \cdot k_{wj}} \qquad \Delta T_{wj} = 7.795 \cdot K$$

$$\Delta T_{wjhigh} = \frac{Q_{loss} \cdot \ln\left(\frac{r_{11}}{r_{10}}\right)}{c \cdot k_{wjhigh}} \qquad \Delta T_{wjhigh} = 7.668 \cdot K$$

c. Temperature at Node 11

$$T_{11low} = T_{10low} - \Delta T_{wjlow} \qquad T_{11low} = 337.567 \cdot K$$

$$T_{11} = T_{10} - \Delta T_{wj} \qquad T_{11} = 368.649 \cdot K$$

$$T_{11high} = T_{10high} - \Delta T_{wjhigh} \qquad T_{11high} = 394.724 \cdot K$$

86

These calculations yield a water channel inner wall temperature of between 64-122 °C. Using the Dittus-Boelter correlation convective heat transfer coefficient of 1012 W/m²K as the upper limit and the Seider-Tate correlation convective heat transfer coefficient of 528 W/m²K as the lower limit, the last resistance in the network can be calculated and a bulk cooling water temperature can be calculated.

6. WATER CHANNEL

a. Convective Heat Transfer Coefficient and Heat Transfer Area

$$h_{low} = 528 \cdot \frac{watt}{m^2 \cdot K}$$

$$A_{htlow} = 0.07 \cdot m^2$$

$$A_{hthigh} = 0.125 \cdot m^2$$

$$h_{high} = 1012 \cdot \frac{watt}{m^2 \cdot K}$$

$$A_{ht} = \frac{A_{htlow} + A_{hthigh}}{2} \qquad A_{ht} = 0.098 \cdot m^2$$

b. Temperature Drop from the Wall to the Bulk Fluid Temperature

$$\Delta T_{wlow} = \frac{Q_{loss}}{A_{ht} \cdot h_{low}} \qquad \Delta T_{wlow} = 56.209 \cdot K$$

$$\Delta T_{whigh} = \frac{Q_{loss}}{A_{ht} \cdot h_{high}} \qquad \Delta T_{whigh} = 29.327 \cdot K$$

c. Bulk Water Temperature

$$T_{bulklow1} = T_{11low} - \Delta T_{wlow} \qquad T_{bulklow1} = 281.357 \cdot K$$

$$T_{bulklow2} = T_{11low} - \Delta T_{whigh} \qquad T_{bulklow2} = 308.24 \cdot K$$

$$T_{bulk1} = T_{11} - \Delta T_{wlow} \qquad T_{bulk1} = 312.439 \cdot K$$

$$T_{bulk2} = T_{11} - \Delta T_{whigh} \qquad T_{bulk2} = 339.322 \cdot K$$

$$T_{bulkhigh1} = T_{11high} - \Delta T_{wlow} \qquad T_{bulkhigh1} = 338.515 \cdot K$$

$$T_{bulkhigh2} = T_{11high} - \Delta T_{whigh} \qquad T_{bulkhigh2} = 365.398 \cdot K$$

These calculations give a bulk cooling water temperature range of 8-92 °C.

C. FROM THE COLLECTOR SLEEVE INWARD

1. STAINLESS STEEL COLLECTOR SLEEVE

a. Thermal Conductivity of Stainless Steel

$$k_{SS} = 12.0 \cdot \left(\frac{watt}{m \cdot K}\right) + 0.01 \cdot \left(\frac{watt}{m \cdot K^2}\right) \cdot T_6 \qquad k_{SS} = 19.268 \cdot \frac{watt}{m \cdot K}$$

b. Temperature Drop Across Collector Sleeve

$$\Delta T_{SSi} = \frac{Q_{loss} \cdot \ln\left(\frac{r_6}{r_5}\right)}{c \cdot k_{SS}} \qquad \Delta T_{SSi} = 10.888 \cdot K$$

c. Temperature at node 5

$$T_5 = T_6 + \Delta T_{SSi} \qquad T_5 = 737.717 \cdot K$$

2. UNREGULATED HELIUM GAP

a. Thermal Conductivity of a Helium Continuum

$$k_{He1i} = 9.376 \cdot 10^{-4} \cdot \left(\frac{watt}{m \cdot K^2}\right) \cdot T_5 - 9.13 \cdot 10^{-7} \cdot \left(\frac{watt}{m \cdot K^3}\right) \cdot T_5^2$$

$$k_{He2i} = 5.5 \cdot 10^{-10} \cdot \left(\frac{watt}{m \cdot K^4}\right) \cdot T_5^3 - 1.264 \cdot 10^{-13} \cdot \left(\frac{watt}{m \cdot K^5}\right) \cdot T_5^4$$

$$k_{Hei} = -9.06 \cdot 10^{-2} \cdot \left(\frac{watt}{m \cdot K}\right) + k_{He1i} + k_{He2i} \qquad k_{Hei} = 0.288 \cdot \frac{watt}{m \cdot K}$$

b. Temperature Drop Across the Unregulated Helium Gap

$$\Delta T_{Hei} = \frac{Q_{loss} \cdot \ln\left(\frac{r_5}{r_4}\right)}{c \cdot k_{Hei}} \qquad \Delta T_{Hei} = 22.382 \cdot K$$

c. Temperature at Node 8

$$T_4 = T_5 + \Delta T_{Hei} \qquad T_4 = 760.099 \cdot K$$

3. ALUMINA INSULATION

a. Thermal Conductivity of Stainless Steel

$$k_{alum1} = 74.9 \cdot \frac{watt}{m \cdot K} - 0.178 \cdot \frac{watt}{m \cdot K^2} \cdot T_4 + 1.75 \cdot 10^{-4} \cdot \frac{watt}{m \cdot K^3} \cdot T_4^2$$

$$k_{alum2} = -7.78 \cdot 10^{-8} \cdot \frac{watt}{m \cdot K^4} \cdot T_4^3 + 1.31 \cdot 10^{-11} \cdot \frac{watt}{m \cdot K^5} \cdot T_4^4$$

$$k_{alum} = k_{alum1} + k_{alum2} \qquad k_{alum} = 10.916 \cdot \frac{watt}{m \cdot K}$$

b. Temperature Drop Across the Alumina Insulation

$$\Delta T_{alum} = \frac{Q_{loss} \cdot \ln\left(\frac{r_4}{r_3}\right)}{c \cdot k_{alum}} \qquad \Delta T_{alum} = 1.784 \cdot K$$

c. Temperature at node 3

$$T_3 = T_4 + \Delta T_{alum} \qquad T_3 = 761.883 \cdot K$$

4. COLLECTOR

a. Thermal Conductivity of Polycrystalline Molybdenum

$$k_{polyMo} = 110 \cdot \frac{watt}{m \cdot K} - 1.5 \cdot 10^{-2} \cdot \frac{watt}{m \cdot K^2} \cdot T_3 \qquad k_{polyMo} = 98.572 \cdot \frac{watt}{m \cdot K}$$

b. Temperature Drop Across the Collector .

$$\Delta T_{coll} = \frac{Q_{loss} \cdot \ln\left(\frac{r_3}{r_2}\right)}{c \cdot k_{polyMo}} \qquad \Delta T_{coll} = 2.051 \cdot K$$

c. Temperature at Node 2

$$T_2 = T_3 + \Delta T_{coll} \qquad T_2 = 763.934 \cdot K$$

APPENDIX D. WATER CHANNEL CALCULATIONS

A.   WATER CHANNEL HEAT TRANSFER AREA

1. Dimensional Constants

$r_{11} = 0.0325 \cdot m$ ----- Inner Cylinder Radius in m

$r_{13} = 0.0425 \cdot m$ ----- Outer Cylinder Radius in m

$z = 0.326 \cdot m$ ----- Water Jacket Length in m

$r_c = 0.005 \cdot m$ ----- Radius of the Flow Guidance Coil

$d_{cl} = 0.075 \cdot m$ ----- Test Stand Diameter to center of the Water Channel in m

$\theta = 13 \cdot deg$ ----- Cant Angle of Flow Guidance Coil in degrees

$N = 6.5$ ----- Number of Revolutions of the Flow Guidance Coil

2. Inner Cylinder Surface Area in m²:

$$A_i = 2 \cdot \pi \cdot r_{11} \cdot z$$

$$A_i = 0.067 \cdot m^2$$

3. Outer Cylinder Surface Area in m²:

$$A_o = 2 \cdot \pi \cdot r_{13} \cdot z$$

$$A_o = 0.087 \cdot m^2$$

4. Surface Area of the Flow Guidance Coil in m²:

$$d_{eff} = \frac{d_{cl}}{\cos(\theta)}$$ ----- Effective Test Stand Diameter based on the Flow Guidance Coil Cant Angle in m

$$d_{eff} = 0.077 \cdot m$$

$$L = N \cdot \pi \cdot d_{eff}$$ ----- Length of the Flow Guidance Coil in m

$$L = 1.572 \cdot m$$

$$C_c = 2 \cdot \pi \cdot r_c$$ ----- Circumference of the Flow Guidance Coil in m

$$C_c = 0.031 \cdot m$$

$$A_c = L \cdot C_c$$ ----- Surface Area of the Flow Guidance Coil in m²

$$A_c = 0.049 \cdot m^2$$

5. **Total Surface Area in Water Channel in m²:**

$$A_t = A_i + A_o + A_c$$
$$A_t = 0.203 \cdot m^2$$

B. HEAT TRANSFER CORRELATIONS

1. Definitions of Physical Properties of Water at 15°C (Welty et al., 1984):

$$\rho = 1000.0 \cdot \left(\frac{kg}{m^3}\right) \qquad \text{----- Density}$$

$$c_p = 4185.0 \cdot \left(\frac{joule}{kg \cdot K}\right) \qquad \text{----- Specific Heat Capacity}$$

$$\mu = 11.6 \cdot 10^{-4} \cdot \left(\frac{kg}{m \cdot sec}\right) \qquad \text{----- Dynamic Viscosity}$$

$$\nu = 11.6 \cdot 10^{-7} \cdot \left(\frac{m^2}{sec}\right) \qquad \text{----- Kinematic Viscosity}$$

$$k = 0.59 \cdot \left(\frac{watt}{m \cdot K}\right) \qquad \text{----- Thermal Conductivity}$$

$$Pr = \frac{c_p \cdot \mu}{k} \qquad Pr = 8.228 \qquad \text{----- Prandtl Number}$$

2. Total Cooling Water Flow Area in m²:

$$A_f = (0.035 \cdot m) \cdot (0.010 \cdot m) - \pi \cdot (0.005 \cdot m)^2$$
$$A_f = 2.715 \cdot 10^{-4} \cdot m^2$$

3. Wetted Perimeter in m:

$$P_w = (2 \cdot 0.035 \cdot m) + \left(2 \cdot \pi \cdot r_c\right)$$
$$P_w = 0.101 \cdot m$$

92

4. Equivalent Hydraulic Diameter in m:

$$D_e = 4 \cdot \frac{A_f}{P_w}$$

$$D_e = 0.011 \cdot m$$

5. Cooling Water Flow Velocity in m/s:

$$V = 0.69 \cdot \left(\frac{gal}{min}\right) \qquad V = 4.353 \cdot 10^{-5} \cdot m^3 \cdot sec^{-1} \qquad \text{----- Measured Volumetric Flow rate}$$

$$v = \frac{V}{A_f}$$

$$v = 0.16 \cdot m \cdot sec^{-1}$$

6. Reynolds Number:

$$Re = \frac{D_e \cdot v \cdot \rho}{\mu}$$

$$Re = 1.48 \cdot 10^3$$

7. Seider-Tate Relation for Laminar Flow:

$$Pe = Re \cdot Pr \qquad Pe = 1.218 \cdot 10^4 \qquad \text{----- Peclet Number}$$

$$\mu_w = 352 \cdot 10^{-6} \cdot \left(\frac{kg}{m \cdot sec}\right) \qquad \text{----- Wall Temperature Fluid Viscosity for 80°C:}$$

$$h_{ST} = \frac{k}{D_e} \cdot 1.86 \cdot \left(Pe \cdot \frac{D_e}{L}\right)^{\frac{1}{3}} \cdot \left(\frac{\mu}{\mu_w}\right)^{0.14}$$

$$h_{ST} = 528.245 \cdot \frac{watt}{m^2 \cdot K}$$

8. Dittus-Boelter Correlation for Fully Developed Turbulent Flow:

$$h_{DB} = \frac{k}{D_e} \cdot 0.023 \cdot Re^{0.8} \cdot Pr^{0.4}$$

$$h_{DB} = 1.012 \cdot 10^3 \cdot \frac{watt}{m^2 \cdot K}$$

93

94

LIST OF REFERENCES

Agnew, P. (1994) Personal Communication, NMERI, Albuquerque, NM, August 1994.

Andrews, J. R. and O. Biblarz (1981) "Temperature Dependance of Gas Properties in Polynomial Form," NPS67-81-001, Naval Postgraduate School, Monterey, CA.

Angelo, J. A. and D. Buden (1985) *Space Nuclear Power*, Orbit Book Company, Malabar, FL.

Angrist, S. W. (1965) *Direct Energy Conversion*, Allyn and Bacon, Inc., Boston, MA.

Baumeister, T., ed. (1978) *Mark's Standard Handbook for Mechanical Engineers*, Eighth Edition, McGraw-Hill Book Company, New York, NY.

El-Genk, M. S. and H. Xue (1993) "Simulation of Fission Heated Thermionic Fuel Elements Using Uniform Electrical Heating," in *Proc. 11th Symposium on Space Nuclear Power and Propulsion*, CONF-940101, M. S. El-Genk, ed., American Institute of Physics, New York, AIP Conference Proc. No. 301, 1: 287-295.

El-Genk, M. S., H. Xue, and C. Murray (1993) "Transient and Load-Following Characteristics of a Fully Integrated Single-Cell Thermionic Fuel Element," in *J. Nuc.Tech.*, 102 (2): 145-166.

El-Genk, M. S. and D. V. Rao (1986) "Heat Transfer Correlations for Low Reynolds Number Flows of Water in Vertical Annuli," Presented at the *American Society of Mechanical Engineers Winter Annual Meeting*, 7-12 December, 1986, Anaheim, CA.

Luchau, D. W. et al. (1993) "Thermionic Fuel Element Test Rig: Testing of Single Cell Thermionic Fuel Element Technology," in *Proc. 11th Symposium on Space Nuclear Power and Propulsion*, CONF-940101, M. S. El-Genk, ed., American Institute of Physics, New York, AIP Conference Proc. No. 301, 2: 1031-1036.

Paramonov, D. V. and M. S. El-Genk (1994) "Steady-State and Transient Analyses of the TOPAZ-II Space Nuclear Power System," UNM-ISNPS-3-1994, Institute for Space Nuclear Power Studies, University of New Mexico, NM.

Peckner, D. and I. M. Bernstein (1977) *Handbook of Stainless Steel*, McGraw-Hill Book Company, New York, NY.

Polansky, G. F., G. L. Schmidt, E. L. Reynolds, E. D. Schaefer, B. Ogloblin, and A. Bocharov (1994) "Utilizing a Russian Space Nuclear Reactor for a United States Space Mission: Flight Qualification Issues," in *Proc. 11th Symposium on Space Nuclear Power and Propulsion*, CONF-940101, M. S. El-Genk, ed., American Institute of Physics, New York, AIP Conference Proc. No. 301, 1: 265-274.

Powell, R. W., C. Y. Ho, and P. E. Liley (1966) "Thermal Conductivity of Selected Materials," National Standard Reference Data Series #8, National Bureau of Standards.

Rasor, N. S. (1991) "Thermionic Energy Conversion Plasmas," in *IEEE Transactions on Plasma Science*, 19 (6): 1191-1208.

Reid, R. C., J. M. Prausnitz, and T. K. Sherwood (1977) *The Properties of Gases and Liquids*, McGraw-Hill Book Company, New York, NY.

Schmidt, G. L., F. Thomè, B. Ogloblin, and V. Sinkevich (1994) "TOPAZ II Non-Nuclear Qualification Test Program," in *Proc. 11th Symposium on Space Nuclear Power and Propulsion*, CONF-940101, M. S. El-Genk, ed., American Institute of Physics, New York, AIP Conference Proc. No. 301, 3: 1185-1192.

Voss, S. S. (1994) "TOPAZ II Design Evolution," in *Proc. 11th Symposium on Space Nuclear Power and Propulsion*, CONF-940101, M. S. El-Genk, ed., American Institute of Physics, New York, AIP Conference Proc. No. 301, 2: 791-802.

Welty, J. R., C. E. Wicks, and R. E. Wilson (1984) *Fundamentals of Momentum, Heat, and Mass Transfer*, John Wiley & Sons, New York, NY.

Wold, S. K., O. L. Izhvanov, V. I. Vibivanets, and G. L. Schmidt (1993) "TOPAZ-II Thermionic Fuel Element Testing," in *Proc. 11th Symposium on Space Nuclear Power and Propulsion*, CONF-940101, M. S. El-Genk, ed., American Institute of Physics, New York, AIP Conference Proc. No. 301, 2: 1025-1030.

Wong, H. Y. (1977) *Heat Transfer for Engineers*, William Clowes & Sons Limited, London.

Wyant, F. J. (1994) Personal Communication, NMERI, Albuquerque, NM, November 1994.

INITIAL DISTRIBUTION LIST

1. Defense Technical Information Center 2
   Cameron Station
   Alexandria, Virginia 22304-6145

2. Library, Code 052 2
   Naval Postgraduate School
   Monterey, California 93943-5101

3. Chairman 1
   Department of Aeronautics and Astronautics, Code AA
   Naval Postgraduate School
   Monterey, California 93943-5106

4. Chairman 1
   Space Systems Academic Group, Code SP
   Naval Postgraduate School
   Monterey, California 93943-5101

5. Professor Oscar Biblarz 2
   Department of Aeronautics and Astronautics, Code AA/Bi
   Naval Postgraduate School
   Monterey, California 93943-5106

6. Professor Ashok Gopinath 1
   Department of Mechanical Engineering, Code ME/Go
   Naval Postgraduate School
   Monterey, California 93943-5100

7. TOPAZ International Program 3
   Attn: Frank Thomè
           Frank Wyant
           Paul Agnew
   901 University BLVD, S.E.
   Albuquerque, New Mexico 87106